




Comprehensive analysis of reservoir quality using microfacies and sedimentary environment characterization: insights from core and petrophysical data in early triassic gas reservoirs of the world's largest gas field

Majid Fakhar¹ · Payman Rezaee¹ · Amir Karimian Torghabeh^{2,3,4} 

Received: 3 December 2024 / Accepted: 29 May 2025
© The Author(s) 2025

Abstract

The central Persian Gulf is of paramount economic importance as it hosts the world's largest gas field. Within this region, the Late Permian Dalan Formation and the Early Triassic Kangan/Upper Khuff Formation act as the primary gas reservoirs. The widespread Early Triassic deposits are significant gas reservoirs not only in the central Persian Gulf but also in the Zagros Mountains of Iran and neighboring Arab nations. As global energy demand escalates, the strategic significance of this region within the hydrocarbon market necessitates a comprehensive study. Despite considerable advancements in petroleum geology and the assessment of reservoir quality, there remains a notable knowledge gap concerning the sedimentary environments and facies characteristics of these formations. An integrated approach that combines sedimentological, petrophysical, and core analysis data is essential for optimizing hydrocarbon exploration and production strategies in these reservoirs. One of the primary challenges facing Triassic gas reservoirs in the central Persian Gulf and the Middle East is the limited availability of gas extraction zones. To overcome the existing limitations, a new zoning was established based on the model of sedimentary environments and the microfacies of the studied succession. The identification of these new zones was conducted through foundational studies of the sedimentary environment, microfacies, core analysis, and petrophysical data. The conducted studies have led to the identification of new areas and an increase in gas production. Five sedimentary environments and twelve microfacies were recognized within the Early Triassic succession. The results show that the shoal environment has the highest reservoir quality, with permeability and porosity of 105.6 mD and 34.1%, respectively, establishing it as the primary reservoir. Furthermore, the tidal environment under Highstand Systems Tract (HST) conditions presents permeability and porosity values of 9.35 mD and 5.3%, introducing it as a newly identified secondary reservoir in this succession. In microfacies analysis, the dolomitic ooid grainstone microfacies demonstrates the highest reservoir quality, exhibits the highest reservoir quality, with permeability and porosity values averaging 329.96 mD and 17.2%, respectively. The ooid grainstone microfacies ranks second in reservoir quality, with permeability and porosity values of 139.45 mD and 13.2%, respectively. Both of these facies were deposited in a shoal environment. Additionally, the coarse-crystalline dolostone facies, resulting from the degradation neomorphism of carbonate sands, ranks third in reservoir quality with 83.78 mD permeability and 6.26% porosity deposited in a tidal environment. The findings of this research can be extrapolated to other carbonate reservoirs deposited in homoclinal ramp environments.

Keywords Reservoir quality · Microfacies · Sedimentary environment · Kangan formation · Persian Gulf · Early Triassic · Porosity · Permeability

Abbreviations

CCAL	Conventional core analysis
FB	Facies belt
GR	Gamma ray
HST	Highstand systems tract
LST	Lowstand systems tracts
MFS	Maximum flooding surface
MF	Microfacies
mD	Millidarcy
PEF	Photoelectric factor
RIPI	Research Institute of Petroleum Industry
TST	Transgressive systems tract
VS	Versus

Introduction

The Early Triassic sedimentary succession in Iran is referred to as the Kangan Formation. This formation corresponds to the upper section of the Khuff Formation in the Arab countries. The sediments within the Kangan Formation constitute some of the largest natural gas reservoirs globally, particularly in the Persian Gulf and its surrounding regions, highlighting its significance in the energy sector (Alsharhan and Nairn 1997; Huc 2005; Zadvinskikh 2019). In addition to the Persian Gulf, Permo-Triassic sediments are recognized as significant hydrocarbon reservoirs in various Middle Eastern countries, including Iran (Dalan and Kangan Formation), Qatar (North field or giant gas field), United Arab Emirates (Thamama Formation), Saudi Arabia (Khuff Formation), and Kuwait (Mujdat Formation), Oman (Khuff and Saih Rawl Formations), Iraq (Makhmour and Zubair Formations), (Alsharhan and Kendall 2003; Warner and Howell 2010; Alsharhan and Nairn 2019; Khadr and El-Wahed 2020; Al-Sharhan and Nairn 2020; Khatib and Sidi 2020; Ameen and Al-Khaldi 2021; Al-Maamoon and Askar 2021; Al-Juboury and Al-Azzawi 2021; Al-Malki and Mclean 2023). A critical challenge in carbonate reservoirs is the accurate assessment of reservoir quality to enhance productivity and ensure the preservation of gas resources. Early Triassic deposits have garnered considerable attention from researchers due to their extensive distribution throughout the Middle East. Most studies focusing on the Early Triassic in this region have primarily addressed the sedimentary characteristics and diagenesis of these sequences (Peyravi 2010; Kavooosi 2011; Nader 2011; Mehrabi 2015; Steiner 2018; Salih 2021). The primary objective of this research is to determine reservoir quality based on facies and sedimentary environments models, which serves as a foundation for the exploration and extraction of hydrocarbon resources. To date, most studies regarding reservoir quality and zoning of this major field have relied on petrophysical data

(Rahimpour-Bonab 2010; Esrafil -Dizaji and Rahimpour-Bonab 2013a, 2013b; Al-Khidir 2014; Mehrabi 2015; Amel 2015; Jafarian 2017; Dehghan Abnavi 2021; Kadkhodaie 2022; Karimian Torghabeh 2022; Kakemem 2021), with less emphasis placed on the sedimentary characteristics, depositional environment, and facies of this vast reservoir. There are several common methods for determining reservoir quality worldwide, each with its own advantages and disadvantages. Typically, petrophysical data are utilized for reservoir quality assessment and zonation. However, results and experience have shown that determining the quality of carbonate reservoirs based solely on petrophysical data can be prone to errors. To accurately assess reservoir quality in a carbonate sequence, the optimal approach is to integrate sedimentological data, petrophysical data, and core analysis. The results of this study indicate that by examining facies and sedimentary environments within a sedimentary succession, combined with petrophysical data and core analysis, it is possible to achieve highly accurate reservoir zonation. The research revealed that the Early Triassic deposits in the central Persian Gulf are characterized by five sedimentary environments and twelve distinct facies. These sedimentary environments produced varying conditions that led to the development of facies with different reservoir qualities. Notably, the ooid grainstone microfacies within the central shoal environment exhibited the highest reservoir quality. Petrographic studies further demonstrated that if the ooid grainstone facies is affected by the phenomenon of dolomitization diagenesis, the reservoir quality significantly enhances. In addition, the dolostone facies with coarse crystals in the intertidal environment also exhibits high reservoir quality. These facies are formed under the influence of magnesium-rich solutions within carbonate sands. Observations indicated that the process of degrading neomorphism diagenesis, resulting in increased intercrystalline porosity, plays a significant role in enhancing the reservoir quality of the Early Triassic succession. Conversely, the massive anhydrite and muddy anhydrite facies possess the lowest reservoir quality and divide the gas reservoir into distinct sections as cap rocks. Zonation based on facies and sedimentary environment models are applicable to all other carbonate reservoirs in the Middle East and globally (Alsharhan and Kendall 2003; Edwards and Fletcher 2012; Khadr and El-Wahed 2020; Salih 2021). It is important to note that the high costs and time-consuming nature of coring constituted significant limitations of this study.

Materials and methods

This research was conducted using petrographic studies, core analysis, and petrophysical data. A total of 628 thin sections were prepared from Kangan Formation cores and stained with Alizarin Red solution to distinguish dolomite from calcite. The cores from the Kangan Formation were analyzed at the Research Institute of Petroleum Industry (RIPI) in Iran. The samples were selected in the range of 10–20 cm. Each sample was analyzed for conventional core analysis (CCAL), permeability, and porosity. Full suite log data was also employed in this research. These logs are acquired at the end of the drilling operation. A full suite log typically includes the gamma ray (GR), resistivity log, density log, porosity log (neutron log), caliper log, and photoelectric factor (PEF) log. Data from these petrophysical logs were used to determine lithology, permeability, porosity, and water and gas saturation. Petrophysical data were analyzed using Petrel and geolog software. Studies on reservoir quality reveal a relationship between permeability and porosity in the reservoir rock. Numerous studies have been conducted based on permeability versus porosity diagrams

(Petunin 2011; AlHomadhi 2014; León Carrera 2018; Abumarah and Nabawy 2021; Ghasemi 2022). In this research, petrophysical data were integrated with petrographic studies to interpret the sedimentary environment and microfacies. To achieve this, two-variable diagrams of permeability versus porosity and histogram diagrams were drawn to assess and interpret the reservoir quality of the sedimentary environments and microfacies. Consequently, permeable and extractable zones were distinguished from impermeable and non-reservoir zones. Of course, it should be noted that by leveraging machine learning algorithms, AI can analyze complex relationships between lithology, porosity, permeability, and reservoir characteristics, enabling the identification of hidden patterns and correlations that enhance reservoir evaluation. This integration allows for a more comprehensive understanding of how sedimentary processes influence reservoir quality, ultimately improving prediction accuracy and informing better decision-making in reservoir management.

Geological setting

The Zagros folded belt is divided into western, central, and eastern sections by the Balaroud and Qatar-Kazerun faults (Falcon 1974; Motiei 1993; Sherkati and Letouzy 2004) (Fig. 1). The Qatar-Kazerun fault, trending from north to south, has acted as a primary controlling factor for the sedimentary patterns and deformation of the region since the Pre-Cambrian period (Murris 1980; Koop and Stoneley 1982; Bahroudi and Talbot 2003; Sepehr and Cosgrove 2004; Bordenave and Hegre 2010). In the eastern part of the Zagros fold, both the offshore and onshore areas are among the most productive hydrocarbon reservoirs in the world. The primary source rock for these regions is likely the Sarachan Formation, dating back to the Early Silurian period and equivalent to the Qusaiba hot shales (Pollastro 2003; Bordenave 2008).

The succession of formations in the studied area, listed from bottom to top, includes: Faraghan, Dalan, and Kangan Formations (Dehram Group); Dashtak and Neyriz Formations (Kazerun Group); Surmeh, Hith, Fahlian, Gadvan, and Darian Formations (Khami Group); and Kazhdumi, Sarvak, Lafan, and Ilam Formations (Bangestan Group) (Fig. 2).

The lateral extension of the Kangan Formation towards the east, along with the Dashtak Formation, transitions into the non-reservoir Khane Kat Formation. This formation extends westward to Lorestan, where its thickness remains relatively constant; however, the thickness of the Dashtak Formation decreases in this direction (Fig. 3) (Motiei 1993, 1995). The Kangan Formation dates back to the Early Triassic period and is situated at a depth of 2.7 km below sea

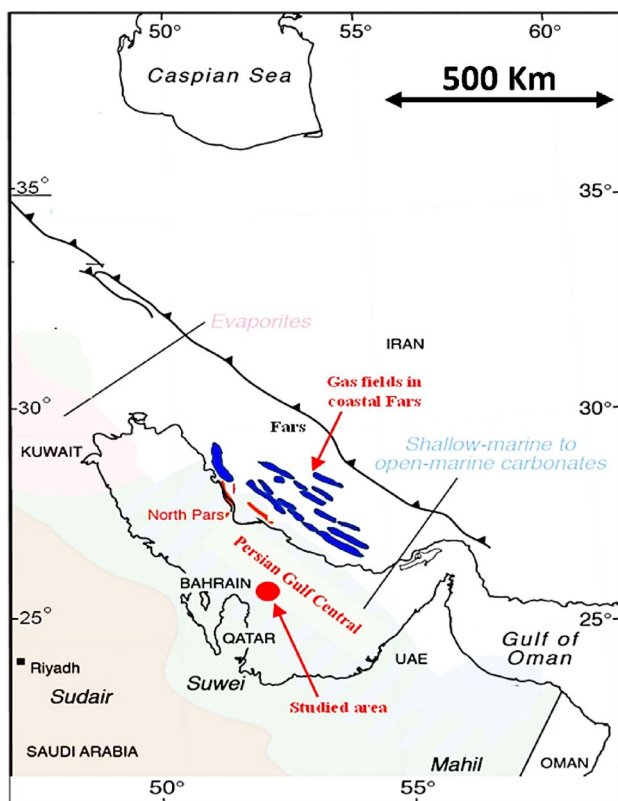


Fig. 1 The central part of the Persian Gulf (offshore) along with the surrounding gas fields located in the onshore region of Coastal Fars. The blue stripes indicate anticlines containing gas reservoirs in the Fars Coastal Basin, and the red circle indicates the location of the world's largest gas field. (adapted from Ziegler 2001)

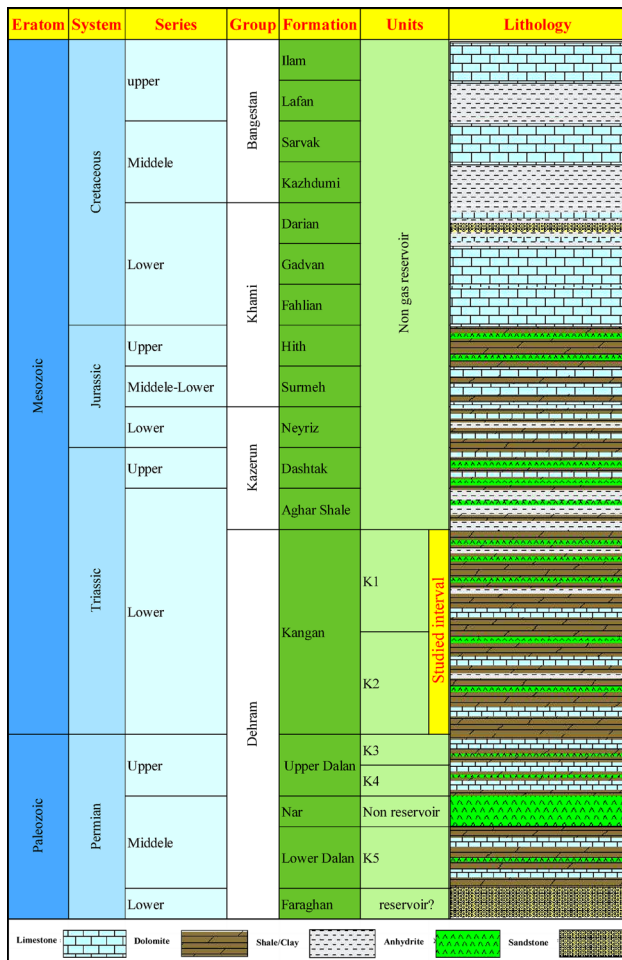
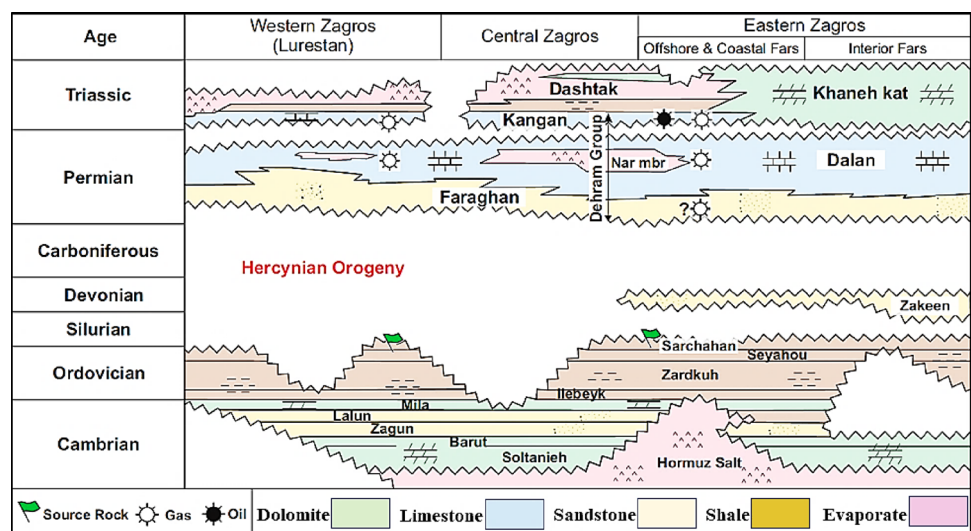


Fig. 2 chronostratigraphy, lithostratigraphy of the Persian Gulf central succession and divided Permo-Triassic reservoir

level, above the Qatar-Fars arch. This formation is located in the northern part of the dome structure. The Qatar arc has developed over several geological periods. The structural evolution of this sequence is linked to the reactivation of Paleozoic faults from the Cambrian period. At the beginning of the Cambrian period, an anticline with an NNE-SSW trend divided the Persian Gulf basin into two parts: the northern and southern salt basins (Al-Husseini 2000). The absence of Cambrian Hormuz series salts above the Qatar arc (the Iranian part of the Persian Gulf) has significantly influenced the geological evolution of the region (Perotti 2011). The Qatar arc is covered by a thick succession of carbonates, which serve as substantial gas reservoirs, along with thin interlayers of evaporites and clay (shale). The Qatar arc emerged at the end of the Triassic to the beginning of the Jurassic and again during the Cretaceous (specifically in the Turonian and Alpine-1 uplift) (Murriss 1980). Uplift of the arc occurred from the early to mid-Eocene and again at the end of the mid-Eocene. The most significant stage of uplift took place during the Late Eocene to Oligocene, coinciding with the Alpine-2 uplift event, resulting from the expansion of the great discontinuity. The subsequent phase of uplift began in the Early Miocene and intensified during the Late Miocene to Pliocene (Perotti 2011).

In the homoclinal ramp environment, research has demonstrated that fluctuations in seawater levels lead to the formation of various depositional environments and distinct microfacies. When seawater levels decline, the connection between open seawater and the lagoonal and intertidal zones is disrupted, resulting in the accumulation of evaporite deposits. Sequence boundaries (S.B.) arise from sea level drop and are established at the conclusion of the highstand systems tract (HST). Conversely, rising sea levels cause facies migration and give rise to maximum flooding surfaces (MFS) in the deeper marine setting. The maximum

Fig. 3 Stratigraphic position of the Kangan Formation laterally and vertically and the surrounding hydrocarbon reservoirs in the Zagros area. (adapted from Motiei 1993)



flooding surface represents the culmination of rising sea levels at the end of the transgressive systems tract (TST). Both the S.B. and MFS intervals exhibit poor reservoir quality (Fakhar 2022).

Discussion.

Analysis of microfacies and sedimentary environment

Primary pore types, pore size expansion, and the reservoir potential of deposited sediments are influenced by microfacies characteristics (Limin 2019) and the sedimentary environment. Additionally, most diagenetic features, particularly early diagenesis, are directly or indirectly associated with microfacies characteristics (Morad 2012; Mahdi and Aqrabi 2018; Boughalmi 2019; Wenju 2020; Fakhar 2024). Studies have shown that the Kangan Formation formed in a

homoclinal ramp environment under a hot and dry climate. Petrographic investigations have identified 12 microfacies across 5 sedimentary environments within the Kangan Formation (Table 1). The following sections will analyze and interpret the facies belts and their corresponding facies

Supratidal facies belt (FB1)

This facies belt corresponds to a depositional environment characterized by extremely low energy and shallow depths during the Early Triassic, typically associated with restricted, hypersaline conditions. The lithology predominantly comprises anhydrite and primary dolomite, which are indicative of evaporitic and hypersaline depositional settings, conditions conducive to the precipitation of sulfate minerals in arid, restricted basin environments (Dunham 1962; Fakhar 2022). These depositional environments are often linked to high evaporation rates exceeding freshwater

Table 1 Facies belts, facies, and their characteristics in the early triassic of the Persian Gulf in the studied area

Facies belt	Facies code	Facies name	Lithology	Describe	Component	Environment	Level of energy	Sedimentary structure	Equal facies		
									Flügel 2010	Wilson 1975	
FB1: Supratidal Flat Facies Belt	MF1	Massive Anhydrite and Muddy Anhydrite	Anhy.	30-100 cm thickness, with shapes: Acicular, Fibrous, radial fibrous, Bladed and Blocky, No fossil	90-100% Anhydrite and/or 0-10% Mud, Crystalline Anhydrite with some mud	Supratidal occasionally intertidal and lagoon, Sabkha, Pond, Evaporate condition and hypersaline	Low	Laminated or aligned structure and wave structure, Chicken wire, Introlitic structure	SMF25	RMF25	FZ9-A
	MF2	Anhydritic Dolomite	Dol., Anhy.	Fine crystalline Dolomite (Primary Dolomite < 10µ) with anhydrite as filled fracture, No fossil	70-80% Dolomite and 20-30% Anhydrite/Gypsum	Supratidal occasionally intertidal, Sabkha, Pond, Evaporate condition and hypersaline	Low	Hard and dense structure, Nodular structure	SMF23	RMF25	FZ8
FB2: Tidal Flat Facies Belt	MF3	Crystalline Dolomite	Dol., Anhy.	Secondary dolomite (> 10µ), Euhedral to subhedral crystalline,	95-100% Dolomite and 0-5% Anhydrite	Tidal flat, Shoal	Moderate	Keystone, Some nodular structure	SMF24	RMF23	FZ8
	MF4	Microbially Facies	Lst., Dol.	This Facies production result of cyanobacteria, filaments of alga, grain of peloids and some evaporate deposits	70-80% Mud from microbial activity, 20-30% Bioclast and pelloid	Environment variation: Intertidal to subtidal, some times lagoon	Low to high	Cotted fabric, microbial matt	SMF20/2	RMF18/23	FZ8
	MF5	Pelo-Ooidal Packstone to Grainstone	Dol., Anhy.	Grain facies dominated with Anhydrite/Micrite cement	40-90% Ooid and peloid, 10-60% Anhydritic cement, 10-20% Micritic cement, <5% Bioclast and intraclast	Intertidal to subtidal and shoal to lagoon	Low to moderate	Keystone, Bioturbation, Burrowing	SMF16	RMF29	FZ8/F9-A
FB3: Lagoonal Facies Belt	MF6	Mudstone to Dolomudstone	Lst., Dol. and/or Anhy.	This facies has a mudstone texture with micro spary dolomite (> 10µ and light color)	60-70% Mudstone texture, 5-40% Microdolomite	Supratidal, Subtidal and Lagoon	Low	Nodular structure, Felted fabric, Scolayots, Burrowing and some times chicken wire (high Anhy.)	SMF23	RMF19/25	FZ8/F9-A
	MF7	Bioclastic, Peloidal Mudstone to Wackestone	Dol., Anhy.	Mudstone texture, Dark color, Secondary Anhydrite as replace of fossil shell and filled space	90-95% Mudstone to Dolomudstone texture with Pelloid and bioclast < 10%	Lagoon, Subtidal	Low to moderate	Nodular structure, Burroing	SMF22/23	RMF18/25	FZ8
	MF8	Pelo-Ooidal Wackestone to Packstone	Dol., Anhy.	High micritization 1 grains and pieces, Anhydrite cement as between grains and filled spaces, Gastropod and bivalve appearance with decrease Anhydrite	10-50% pelloid and ooid, 10-15% Anhydrite cement also can be seen < 10% Interclast and bioclast	Lagoon, leeward shoal, tranzitional tidal to shoal	Moderate to high	Turbation and bioturbation	SMF16	RMF14	FZ8
FB4: Shoal Facies Belt	MF9	Bioclast, Intraclast, Pello Ooid Grainstone	Dol., Anhy.	Submaturity in grains, Micritization as rime of grains to all grains also micrite can be seen as between grains cement	50-70% Ooid and pelloid, 15-20% Anhydrite cement, <10% Anoid	Tranzitional shoal to leeward and/or seaward, Tranzitional tidal to lagoon	Moderate to high	Turbation and bioturbation	SMF13	RMF30	FZ6
	MF10	Ooidal Grainstone	Lst., Dol.	Bigest and tangentially ooid in all of facies, This ooids can be seen with open marin rim cement, High properm propertice in all of facies with significant amount of oil show	90% Ooid and 10% grapestone intraclast	Shoal	High	Grapestone, Spalotite	SMF15	RMF29	FZ7
	MF11	Bioclastic, Intraclast, Ooid Grainstone	Lst., Dol.	Submatur to imature in grains with big intraclast to 2cm, Some micritization as rime of grains with solution inside grains	50-60% Ooid, 20-30% Intraclast, 10-20% Bioclast	Leeward and seaward shoal	High to moderate	Turbation and bioturbation	SMF18	RMF27-30	FZ6-7
FB5: Open Marine Facies Belt	MF12	Shaly Mudstone to Bioclastic Mudstone to Wackestone	Lst	Fine grain carbonate deposite with organic or chemical origin and some bioclast with thin and delicate shell	90% Matrix as mudstone, 10% Allocem as fine ooid and bioclast	Backward shoal, Open marin	Low	Fissility structure	SMF10	RMF5/7	FZ4-5

inflow, resulting in a significant concentration of salts and carbonate minerals under conditions of stagnation and limited circulation. The microfacies associated with this facies include laminated anhydrite and mudstone microfacies, which reflect rapid evaporation and low-energy conditions prevalent in supratidal zones (Flügel 2010). Such environments are key to understanding the genesis of extensive evaporite deposits and their relationship with adjacent carbonate systems, providing vital insights into paleoenvironmental dynamics and sequence stratigraphy of the region.

Massive and muddy anhydrite facies (MF1) This facies is significant within the belt as it divides the Kangan Formation reservoir into several parts due to its impermeability. Massive anhydrite crystals are observed in various forms, including microcrystalline, blocky, bladed, and radially fibrous (Fig. 4A). Occasionally, more than 30% mud is present alongside the anhydrite. The combination of mud with anhydrite can result in chicken wire structures and enterolith structures (Fig. 4B, C). Occasionally, tectonic forces create stresses in these microfacies that result in linear structures (Fig. 4D). This microfacies typically forms in supratidal environments, such as sabkhas and small evaporation ponds. However, it can also be found in tidal and lagoon environments under hypersaline conditions, appearing as pure anhydrite/gypsum or in combination with some mud (e.g., Kendall and Skipwith 1969; Insalaco 2006; Aleali 2013; Fakhar 2022).

Anhydritic dolostone facies (MF2) These dolomites are formed through evaporative dolomitization. The dolomites in this section typically appear as primary dolomites, resulting from primary diagenesis in a hypersaline environment rich in Mg^{2+} (Fig. 5F). While this microfacies primarily forms in supratidal environments, it can also deposit in central lagoons and during the final stages of disconnection from seawater. Generally, these microfacies develop in calm, low-energy environments (Wilson 1975).

Tidal flat facies belt (FB2)

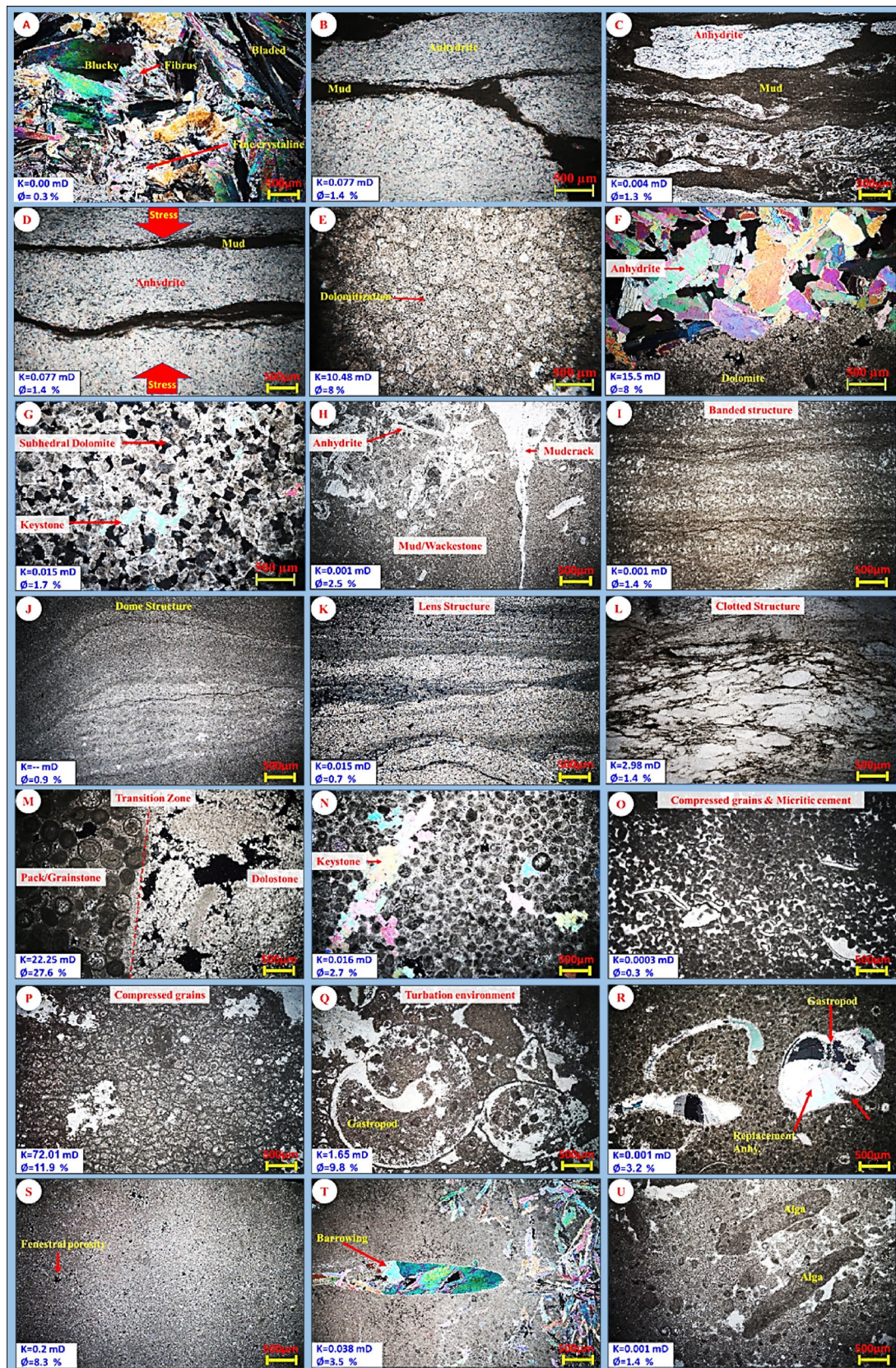
This environment is situated between the supratidal environment and the lagoon environment. Energy levels in the tidal environment vary considerably, ranging from high-energy to calm, low-energy settings. Dolomites in this environment are often formed through the *seepage reflux model* (Fig. 4E). Additionally, under highstand systems tract (HST) conditions, anhydrite/gypsum may also form in the tidal environment (Fakhar 2022) (Fig. 4F). Most dolomites in the Kangan Formation are secondary and occur

Fig. 4 **A** Massive anhydrite (MF1) with sparse and isolated evaporate crystals. **B** Muddy anhydrite (MF1) exhibiting a chicken wire structure. **C** Muddy anhydrite (MF1) with an introilite structure. **D** Muddy anhydrite (MF1) displaying a linear structure. **E** Crystalline dolostone (MF3) formed on a seepage reflux model. **F** Anhydrite/gypsum crystals adjacent to dolomite in a tidal environment. **G** Keystone structure formed with anhydrite/gypsum between dolomite crystals. **H** Mud crack structure observed in a tidal environment due to retrograde water from the beach. **I** Flat stromatolite boundstone resulting from microbial activity (MF4) formed in a tidal environment. **J** Stromatolite boundstone exhibiting a dome structure. **K** Stromatolite boundstone with a lens structure. **L** Thrombolite microfacies resulting from microbial activity with a clotted fabric. **M** Transitional zone between dolostone and pelo-oidal pack to grainstone. **N** Fine ooids (<1 mm) and a keystone structure in pelo-oidal pack to grainstone. **O** Compaction grains with micrite and anhydrite cement in pelo-oidal pack to grainstone. **P** Compaction and unsorted grains with an anhydrite patch in ooidal pack to grainstone. **Q** Turbation in lagoon facies with intraclasts, bioclasts, peloids, and ooid grains in micritic cement in bioclastic packstone. **R** Bioclast and peloid grains in micritic cement with boring trace fossils in bioclastic packstone. **S** Mudstone to dolomudstone with fenestral porosity in a lagoon environment. **T** Bioturbation and burrowing trace fossils in anhydrite mudstone to dolomudstone microfacies, filled with anhydrite cement. **U** Bioclastic peloid mudstone to wackestone with algal fossils in a lagoon environment

as replacements, with a smaller amount present as cement (Kadkhodaie-Ilkhchi 2018). In shoal environments, dolostone may also form from the dolomitization of ooid grains (Wilson 1975), which significantly enhances reservoir quality. The structures found in this environment include keystone structures and mud crack structures. The keystone structure refers to the presence of anhydrite/gypsum filling the spaces between coarse dolomite crystals (dolospirite). Mud crack structures typically develop in areas of tidal flats that are more frequently exposed (Fig. 4G, H). The characteristics of the facies belt and tidal microfacies are detailed in Table 1, and this belt comprises the following facies.

Crystalline dolostone microfacies (MF3)

This facies develops under relatively deeper depositional conditions with lower salinity compared to the anhydrite-dolostone microfacies and may exhibit lateral and vertical facies transitions or alternations (Flügel 2010). Anhydrite cement is infrequently observed within this facies, indicating limited evaporation or episodic deposition. In the crystalline dolostone microfacies (MF3), dolomite occurs predominantly as a diagenetic secondary mineral, characterized by coarse euhedral to subhedral crystals, reflecting extensive recrystallization processes and diagenetic overprinting typical of deeper, more modified carbonate environments (Fakhar 2024).



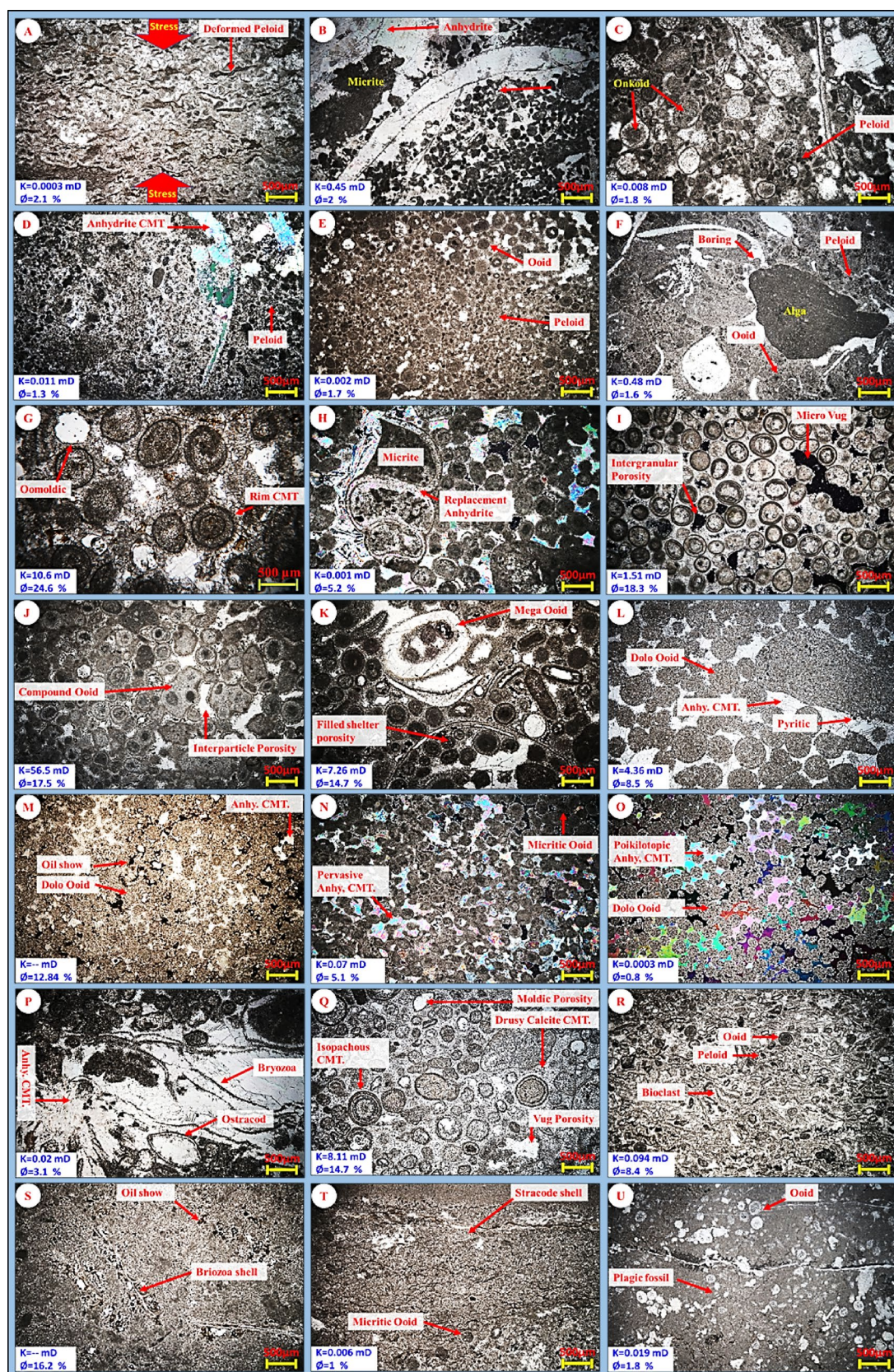


Fig. 5 **A** Peloidal wackestone facies: a flow structure is created due to stress and deformation of peloid grains. **B** Bioclastic peloid pack to grainstone (MF8): exhibiting replacement features, pore filling, and pervasive anhydrite cement. **C** Oncoidal bioclast intraclast pelo-ooid pack to grainstone (MF8): characterized by algal filaments and micritization. **D** Bioclastic peloid wack to packstone (MF8): found in a lagoon environment adjacent to the shoal. **E** Peloidal Packstone (MF8): formed in the transitional zone between lagoon and shoal. **F** Bioclastic intraclast pelo-ooid packstone (MF8): contains algae and boring trace fossils. **G** Ooidal grainstone (MF10): notable for its rim cement and oil shows. **H** Bioclastic intraclast ooid grainstone (MF9): located in the transitional zone between shoal and lagoon, characterized by pervasive and replacement anhydrite cement. **I** Ooidal grainstone (MF10): features vuggy and intercrystalline porosity. **J** Ooid grainstone (MF10): contains compound ooids, indicating alternating periods of low and high energy. **K** Bioclastic ooid grainstone (MF11): indicative of high energy in a turbation environment. **L** Dolomitic intraclast ooid grainstone (MF11): exhibits pore filling, pervasive anhydrite cement, and traces of pyrite. **M** Dolomitic ooid grainstone (MF10): contains oil as pore-filling intergranular porosity. **N** Anhydritic ooid grainstone (MF10): characterized by pervasive anhydrite cement. **O** Anhydritic ooid grainstone (MF10): exhibits poikilotopic anhydrite cement. **P** Bioclastic ooid pack to grainstone (MF11): contains ostracod and bryozoan fossils with a seaward shoal indication. **Q** Intraclastic pelo-ooid grainstone (MF11): features unsorted grains, indicating a turbation environment and TST of sequence stratigraphy. **R** Bioclastic intraclast pelo-ooid pack to grainstone (MF12): found in the transitional zone between shoal and open marine environments. **S** Bioclastic mud to wackestone (MF12): contains bryozoan debris with oil shows. **T** Bioclastic mud to wackestone (MF12): contains ostracod debris and small micritic ooid grains. **U** Bioclastic ooid wackestone (MF12): represents the transition from shoal to open marine, containing some pelagic fossils

Microbial facies (MF4)

These facies result from microbial activity and are often composed of mud generated by organisms such as cyanobacteria, algae filaments, peloid grains, and some evaporative deposits. In the Kangan Formation, these facies are observed in two distinct forms (Fakhar 2022). (a) *Stromatolite Boundstone Microfacies*: This microfacies appears as bands with light and dark coloration. It can exhibit various structures, including flat, domed, and conical shapes (Fig. 4I, J, K). (b) *Thrombolite Microfacies*: This microfacies is observed as a key bed in the lower part of the Kangan Formation, located just above the boundary with the upper Dalan section, with thicknesses ranging from several centimeters to several tens of centimeters. While both stromatolite boundstone and thrombolite facies are formed from algal structures, thrombolites are characterized by the absence of layering (lamination) and the presence of a clotted fabric (Fig. 4L). Moreover, this facies is located at the base of the Kangan Formation, observed 2 to 3 m above the boundary of biological extinction (Tavakoli 2016). The formation environments for this facies are diverse, with its primary origin in the tidal environment as microbial mats (Esrafil-Dizaji and Rahimpour-Bonab 2009). Additionally, thrombolites form in subtidal and lagoon environments,

developing under conditions that range from calm to chaotic, often accompanied by bioturbation (Kershaw 2012). In the studied area, this microfacies is prominently observed in the tidal belt.

Pelo-Ooidal packstone to grainstone microfacies (MF5)

This facies forms in the energetic parts of the tidal belt. It features keystone pores filled with anhydrite cement, relating it to tidal and subtidal environments where tidal fluctuations trap air bubbles in small allochem grains (Flügel 2010). The presence of packstone to grainstone microfacies, characterized by ooid grains, micritic cement, and rounded intraclast fragments, also indicates a tidal environment (Sabouhi 2019). Pelo-ooidal grainstone microfacies, characterized by anhydrite cement and some dolomitization, indicate tidal and subtidal conditions (Insalaco 2006; Abdolmaleki 2016). This microfacies is less commonly found in intertidal, lagoon, and shoal to lagoon environments (Wilson 1975; Flügel 2010). Occasionally, due to rapid sea level rise, both the depth and energy in the tidal environment increase. Under these conditions, an immediate transition from dolostone microfacies to pelo-ooidal grainstone and/or packstone microfacies is observed (Fig. 4M). The features of the pelo-ooidal grainstone and/or packstone microfacies in the tidal environment include: (a) The presence of small ooid grains with sizes smaller than 0.25 mm (Fig. 4N). (b) Anhydrite observed in the form of keystones among the ooid grains (Fig. 4N). (c) Compression of ooid grains within the anhydrite cement (Fig. 4O). (d) Ooid grains embedded in anhydrite and micritic cement (Fig. 4O). (e) Compaction with poorly graded bedding of grains, accompanied by patches or nodules of anhydrite (Fig. 4P).

Lagoonal facies belt (FB3)

A lagoon is an environment that is separated from the open marine area by a natural barrier (shoal environment). This environment is enclosed between the tidal belt and the shoal. In the transgressive systems tract (TST) of the sequence, the lagoon is fed with water from the open marine. Key features of this environment under TST conditions include turbation, low salinity, and a high diversity of biological fauna (Fig. 4Q). These conditions can enhance the reservoir quality to some extent (Fakhar 2022). In HST conditions, the lagoon environment becomes disconnected from the open marine. When sea level drops and the lagoon is isolated from the open marine due to evaporation, a hypersaline environment forms. In this setting, anhydrite/gypsum (evaporite minerals) are deposited as patches or masses. The most significant features of the lagoon environment in HST conditions include the micritization of allochems and the

replacement of anhydrite cement in fossil shells. Additionally, a significant amount of pellet grains, along with gastropod and bivalve fossils featuring thick shells and *boring trace fossils*, is observed in the lagoonal facies belt (FB3) (Fig. 4R). The lagoon environment in the Kangan Formation comprises the following facies.

Mudstone to dolomudstone microfacies (MF6)

In the deeper parts of the lagoon environment, facies are observed as mudstone to dolomudstone microfacies within a subsidence environment. This environment contains oxygen-poor water, and the mudstone to dolomudstone microfacies is typically observed as massive (Fig. 4S). These microfacies can also form as layers in shallower lagoon environments (Insalaco 2006). When this microfacies is associated with anhydrite, it often exhibits a dolomitic lithology and includes molds, nodules, and anhydrite veins deposited in hypersaline lagoons and ponds (Warren 2006). *Burrowing trace fossils* are sometimes observed in this microfacies, which may be filled with anhydrite cement during the post-formation phase (Fig. 4T).

Bioclastic, peloidal mudstone to wackestone microfacies (MF7)

This microfacies is often accompanied by traces of bioturbation and is deposited in the low-energy environment of the lagoon (Abdolmaleki 2016). Blue-green algae fossils are also observed in the wackestone microfacies of the lagoon section (Fig. 4U), indicating the TST sequence of the lagoon environment and the tolerable salinity for the growth of these organisms. When the connection between the lagoon and the open marine is severed, the restricted lagoon environment becomes saltier due to water evaporation. As a result, its organisms gradually decrease and eventually disappear. Under high salinity conditions, the wackestone lacks living organisms, with some peloids typically observed within them. In the presence of tectonic stress, a flow structure is formed, appearing oriented (Fig. 5A).

Pelo-Ooidal wackestone to Packstone microfacies (MF8)

This microfacies develops in the lagoon environment with a limited and specific fauna (Shakeri 2021). The observed fauna in the lagoon belt, in order of frequency, includes gastropods, bivalves with thick shells, and blue-green algae. These are present when the salinity of the lagoon does not reach hypersaline levels. The pelo-ooidal wackestone to packstone microfacies is commonly found in the environments of the inner ramp boundary (Flügel 2010). The boundary of the inner ramp includes tidal to lagoon and

shoal to lagoon environments. In these higher-energy settings, wackestone to packstone microfacies are observed. The components of this microfacies include peloids, allochems, and sometimes oncoids, along with micritic and/or anhydrite cement (Fig. 5B, C). The dominant grain facies of the lagoon environment (packstone) are typically found at the edges of the lagoon and along its borders with tidal and shoal environments. Usually, from the center of the lagoon toward the shoal, the amount of peloid grains increases (Fig. 5D). During sea storms, the high energy of the shoal environment in the TST part of the sequence (during sea-level rise) can result in some ooid grains being transported into the lagoon environment, leading to the formation of dominant grain facies (Fig. 5E). Under TST conditions, the lagoon environment becomes suitable for biological fauna, resulting in an increase in their numbers (Fig. 5F). The microfacies of the lagoon belt and their characteristics are summarized in Table 1.

Shoal facies belt (FB4)

The shoal belt is located between the lagoon environment and the open marine. It represents the highest energy area in ramp environments. One of the prominent characteristics of the shoal environment is the presence of grainstone microfacies (Fig. 5G). The shoal facies belt can be divided into three smaller sub-environments: leeward shoal (toward the lagoon), central shoal, and seaward shoal (toward the open marine). These grainstone microfacies are typically found in high-energy environments such as shoals and platform margins, where wave and current action inhibit fine sediment accumulation (Flügel 2010).

Bioclast, intraclast, Pelo-Ooid grainstone (MF9)

This microfacies is formed in the shoal area toward the lagoon. It exhibits common characteristics of both the shoal and lagoon environments, including micritization and dolomitization of grains, anhydritization, the presence of lagoon index fossils (such as gastropods), and some peloids (Fig. 5H). Significant micritization of allochems, the poor maturity of grains, the presence of anhydrite cement, and a small amount of oncoids indicate a low-energy environment (Flügel 2010) and reflect this microfacies's transition from the shoal toward the lagoon (transition zone environment). Overall, the formation of this microfacies occurs in the shoal towards landward.

Ooid grainstone microfacies (MF10)

This facies is formed in the central shoal, which represents the most energetic part of the ramp. The ooid grainstone

microfacies is typically made up of concentric grains larger than 0.5 mm (ooid grade 3 type) (Flügel 2010). Additionally, this microfacies exhibits very good maturity, indicative of the shallow and energetic environment characteristic of the central part of the shoal (Flügel 2010) (Fig. 5I). The presence of grainstone microfacies and the low amount or absence of mud further suggest a high-energy environment (Tucker 2009). This microfacies typically forms on the inner ramp, including bar sections, ridge channels, and shoals, as well as shallow tidal areas inclined toward the shoal (Flügel 2010). Additionally, ooid grainstone can also develop in the central part of the shoal and in open marine environments (Shakeri 2021). The presence of micrite coatings around ooids (Hossein Yar and Rahimpour Bonab 2011) and the formation of compound ooids (Flügel 2010) indicate alternating low and high energy in this environment (Fig. 5J). It is important to note that due to the dominance of grains in this facies, the energy of the environment was generally high. Sometimes, the energy in the environment is so high that ooids break, and their fragments serve as nuclei for very large ooids or mega-ooids (Fig. 5K). Selective dolomitization is highly developed in the ooid grainstone microfacies, with ooid grains typically undergoing this process. During diagenesis, anhydrite cement fills the empty spaces inside and between the grains (Fig. 5N). When the ooid grainstone microfacies of the shoal is influenced by Mg^{+2} rich solutions, grains are partially or completely transformed into dolomite due to the process of degrading neomorphism (Fig. 5O). After the deposition of the shoal belt, if the environment is affected by sulfate-rich hypersaline solutions, the empty spaces between intergranular or intragranular ooid grains are filled with pervasive anhydrite and/or poikilotopic cement. Furthermore, the grains can be replaceably filled with anhydrite under the influence of hypersaline solutions (Fig. 5P,Q).

Bioclastic, intraclast, ooid grainstone microfacies (MF11)

This microfacies is formed in the seaward shoal (shoal toward the open marine) and exhibits characteristics common to both shoal and open marine environments. Key features of this microfacies include smaller ooid grains, micrite, and calcified ooids. The bioclastic, intraclast, and ooid grainstone contain typical open marine fauna, such as thin-shelled bivalves, algal filaments, ostracoda, bryozoans, and occasionally echinoderms (Fig. 5L). This microfacies can also develop in the central part of the shoal and in open marine environments (Shakeri 2021). Another feature of the seaward shoal environment is the presence of low Mg calcite allochems (with subhedral and/or euhedral crystals), likely resulting from the conversion of high Mg calcite allochems and aragonite (Fig. 5M). The characteristics of the

facies belt and the microfacies of the shoal are summarized in Table 1.

Open marine facies belt (FB5)

The seaward region of the shoal, which is part of the outer ramp, becomes deeper and less energetic as it moves away from the central shoal. The transitional zone between the shoal and open marine environments includes grainstone to packstone microfacies with small ooid grains. Occasionally, peloids and micritic intraclasts are observed, along with calcite cement and, rarely, anhydrite (Fig. 5R). The presence of fossils such as claria bivalves, ostracods, bryozoans, and echinoderms indicates an open marine environment in this microfacies (e.g., Shakeri 2021; Fakhar 2022). Special fauna, including echinoderms, thin-shelled bivalves, and algal filaments, along with proximity to the ooid grainstone facies and the absence (or minimal presence) of anhydrite, are indicators of the outer ramp (Aleali 2013) (Fig. 5S, T). In areas where the microfacies is predominantly composed of mudstone to shaly mudstone sediments, it is associated with the deeper environment of the carbonate ramp (outer ramp) (Hossein Yar and Rahimpour Bonab 2011). In the open marine environment, following the shoal transitional zone, microfacies consist of shaly mudstone and mudstone to bioclastic mudstone microfacies (MF12). Occasionally, during sea storms, ooid grains from the shoal environment may migrate considerable distances and be found in the mud facies of the open marine outer ramp (Fig. 5U). The features of the microfacies in the open marine are summarized in Table 1.

Sedimentary environment model and reservoir quality analysis in the central part of the Persian gulf

Carbonate reservoirs exhibit complex pore systems that are influenced by biological origins and significant chemical reactions occurring within their sedimentary environments (Flügel 2010; Moore 2013). Several factors influence reservoir quality within sedimentary environments, including environmental energy, depth, salinity, water composition, and the conditions of marine transgression or regression. Among these, environmental energy and the concentration of salts or soluble elements play a particularly significant role in determining sediment reservoir quality. Higher energy environments typically result in lower clay content, leading to the formation of coarser, granulated sediments. Therefore, there is a direct relationship between environmental energy and reservoir quality. Conversely, increased salinity levels are associated with higher occurrences

of evaporite deposits, indicating an inverse relationship between reservoir quality and saline concentrations. Furthermore, dominant grain facies are more likely to be deposited in high-energy environments, while evaporite facies tend to form in low-energy, high-concentration settings. The sedimentary environments of the Kangan Formation in the central region of the Persian Gulf include the following: supratidal belt (5.6%), tidal flat belt (32.84%), lagoon belt (25.56%), shoal belt (30.92%), and open marine belt (5.05%) (Fig. 6).

Supratidal environment

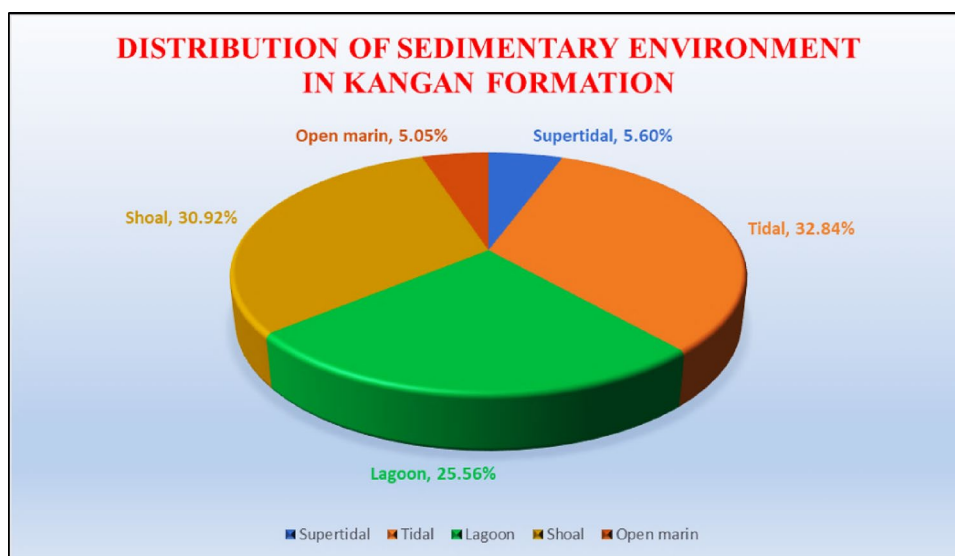
This section exhibits the lowest porosity and permeability within the Early Triassic succession of the studied area. The sediments of the supratidal environment act as a barrier, dividing the Kangan Formation into several permeable and extractable reservoir segments. The lithology of this section predominantly consists of massive anhydrite and muddy anhydrite (MF1), with thin layers of dolomite and calcite also present within the anhydritic dolostone (MF2) (Fig. 6, 7). The anhydrite section of this belt demonstrates very low permeability and porosity. In contrast, the dolomite and calcite sections exhibit open and semi-filled fractures, which possess higher permeability and porosity (Table 2). The permeability versus porosity diagram for this belt reveals three distinct areas: (a) a permeability range of 1–28 mD and a porosity range of 0.001–1.4%, associated with thin dolomite layers that feature open to semi-open fractures, often filled with cemented anhydrite (Fig. 8A). (b) The permeability range is between 0.001 and 0.024 mD, with a porosity range of 0.4 to 1.8%, corresponding to thin layers of dolomite and calcite without fractures, featuring a small amount of intercrystalline porosity (in dolomite). In this section, interparticle porosity results from dissolution phenomena.

Dissolution porosity arises from surface exposure due to sea level drops and the emergence of layers from underwater conditions, as well as meteoric diagenesis (Fakhar 2024) (Fig. 8A). (c) The evaporite zone predominantly consists of anhydrite/gypsum (with or without mud), forming the major part of this belt, characterized by permeability < 0.2 mD and porosity < 0.4% (Fig. 8A). The histogram of permeability in the supratidal environment reveals that the highest frequency corresponds to the range of 0–3.7 mD, which is associated with primary dolomites featuring micro-fractures filled with anhydrite cement (Fig. 8B). Similarly, the histogram of porosity indicates that the highest range of porosity (over 70%) is found within the 0–0.4% range, particularly in dolomites contaminated with anhydrite (Fig. 8C). The supratidal environment lacks reservoir quality and serves primarily as caprock in carbonate reservoirs.

Tidal environment

The secondary dolomite section, characterized by the absence of anhydrite cement (MF3: crystalline dolostone), is introduced as the secondary reservoir of the Kangan Formation (Table 2). Core analysis and petrographic studies indicate that less than 10% of this succession exhibits acceptable reservoir quality. The secondary reservoir in the tidal environment yields a lower amount of hydrocarbon production compared to the primary reservoir situated in the shoal environment of the Kangan Formation. Petrographic investigations indicate that the reservoir component of the tidal environment consists of secondary dolomites formed through the *seepage reflux model*. The predominant type of porosity is intercrystalline, along with open to semi-open fractures. The high permeability in this section is attributed to these open fractures. The formation and preservation of secondary dolomite in tidal environments are heavily

Fig. 6 Distribution of different ramp environments in the succession of the Kangan Formation in the central part of the Persian Gulf



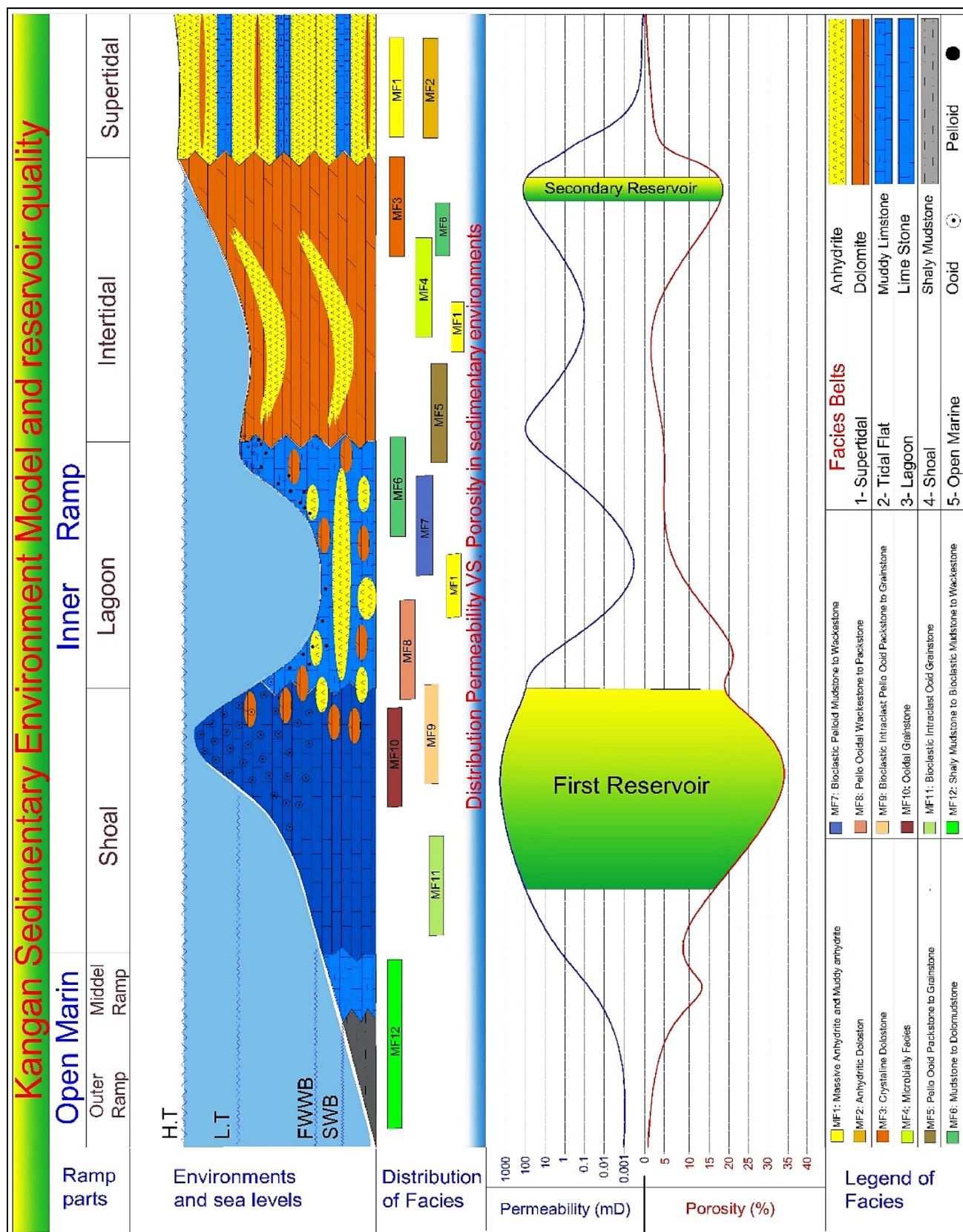


Fig. 7 Sedimentary environment model and reservoir quality of the Kangan Formation during the Early Triassic in the central part of the Persian Gulf, as observed in the study area

Table 2 Minimum, maximum, and average values in different environments of the Kangan Formation in the central part of the Persian Gulf

Environment	Permeability(mD)			Porosity%		
	Average	Max	Min	Average	Max	Min
Supertidal	1.086	29.56	0.001	0.60%	1.80%	0.001%
Tidal	9.35	623.50	0.01	5.30%	24.50%	0.010%
Lagoon	3.37	101.02	0.001	5.90%	18.90%	0.200%
Shoal	105.6	2,255.50	0.1	12.50%	34.10%	0.200%
Open marin	2.52	119.20	0.001	1.90%	18.80%	0.010%

influenced by the interplay of chemical diagenesis, fluid flow, and fracture development, within the context of carbonate reservoir distribution in tidal channel settings (Xu 2022). The porosity versus permeability diagram for the tidal belt reveals three distinct regions concerning reservoir quality (Fig. 8D). (a)*High permeability and porosity area* (Kangan secondary reservoir): This area exhibits a permeability range of 15–623 mD and a porosity range of 11–18%, associated with secondary dolomites that possess high intercrystalline porosity and open to semi-open fractures. (b)*Zone of high porosity and low permeability*: This zone features porosity between 8 and 14% and low permeability ranging from 0.1 to 1 mD, corresponding to secondary dolomites where pore connectivity is disrupted by anhydrite cement. (c)*Zone without reservoir quality*: Characterized by permeability levels of 0.001–0.1 mD and porosity ranging from 0.001 to 5%, this zone is related to intense cementation by anhydrite cement and contains the highest sample abundance (Fig. 8D). The histogram of permeability in the tidal environment indicates that the highest permeability range is 0–7.1 mD, associated with the microbial facies (MF4), which exhibit bioturbation along with interparticle and intraparticle porosities (Fig. 8E). Additionally, the histogram of porosity for the tidal environment reveals that the maximum porosity range is 0–2.3%, corresponding to the aforementioned microbial facies (Fig. 8F).

Lagoon environment

This environment, indicates deposition in a low-energy, shallow lagoonal environment with limited marine connection (Wilson 1975; Hine 1977; Tomašových 2004). The dominance of peloids and the presence of bioclasts suggest sedimentation within a sheltered, enclosed setting with minimal biotic diversity, consistent with a restricted lagoonal depositional model. These microfacies are indicative of deposition on a carbonate shelf protected by high-energy shoals, forming a barrier at the platform margin, facilitating the development of a broad lagoon with limited open marine influence (Schlager 2005). The lithology of this area

consists of argillaceous limestone, anhydrite nodules and veins, and thin layers of dolomite (Fig. 7). Overall, this area exhibits low reservoir quality and is considered unextractable in terms of production (Table 2). Notably, relatively higher values of permeability (up to 100 mD) and porosity (28%) are observed in the lagoon as it transitions toward the shoal environment, particularly in the TST (Transgressive Systems Tract) stage of the sequence (Table 2). The diagram of permeability versus porosity for the lagoon environment reveals three distinct regions: (a)*High permeability region with low to medium porosity*: This region, characterized by permeability levels of 5–100 mD and porosity ranging from 0.8 to 6%, corresponds to the dolomite section, which features open to semi-open fractures (Fig. 8G). (b)*High porosity area with low to medium permeability*: This region exhibits porosity between 7.4 and 27.9% and permeability levels of 0.1–22.6 mD, encompassing argillaceous limestone with high bioturbation activity. This area features dolomite lithology characterized by interparticle and intraparticle porosities. Thin veins of dolomite exhibit good intercrystalline porosity; however, there is a lack of connectivity between the pores (Fig. 8G). (c)*Low permeability and porosity area*: This region has permeability values of less than 1.7 mD and porosity levels below 6.9%, including mudstone, wackestone, and packstone microfacies, which contain significant amounts of anhydrite and micritic cement (Fig. 8G). The histogram diagrams for permeability and porosity in this environment indicate that the highest permeability corresponds to the range of 0–1.66 mD, while the highest porosity range is between 0.2 and 4.2%, associated with mudstone microfacies to peloid wackestone (MF7). These diagrams demonstrate very low fenestral and intercrystalline porosities, accompanied by anhydrite cement (Fig. 8H; Fig. 9I).

Shoal environment

The high reservoir quality in the shoal environment is primarily controlled by the development of ooid grainstone and dolomitization, which enhance porosity and permeability.

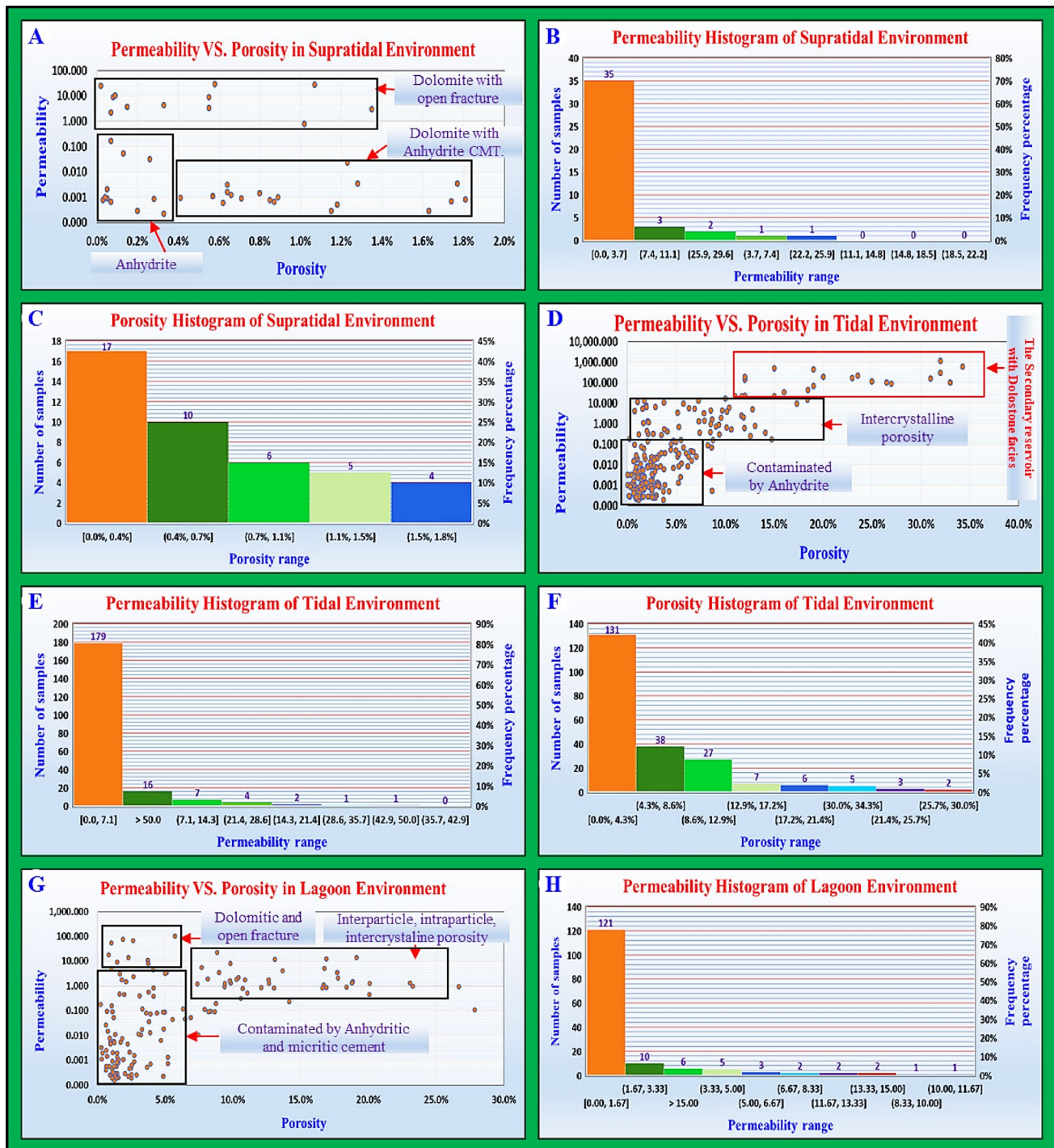


Fig. 8 Permeability versus porosity and histogram diagrams for supratidal, intertidal, lagoon, and shoal environments within the Kangan Formation, analyzing their reservoir quality

However, cementation processes, especially by anhydrite, can significantly reduce effective porosity and impede fluid flow, demonstrating the importance of diagenetic factors in reservoir assessment. These microfacies trends highlight the critical role of depositional and diagenetic controls in optimizing hydrocarbon extraction strategies in carbonate

platform settings (Wilson 1975; Tucker 2009; Flügel 2010; Reijers 2012). The highest reservoir quality of the Kangan Formation is associated with this environment, featuring an average permeability of 105 mD and a porosity of 12.5% (Table 3). The dominant facies in this environment is ooid grainstone (MF10), which exhibits very high intergranular

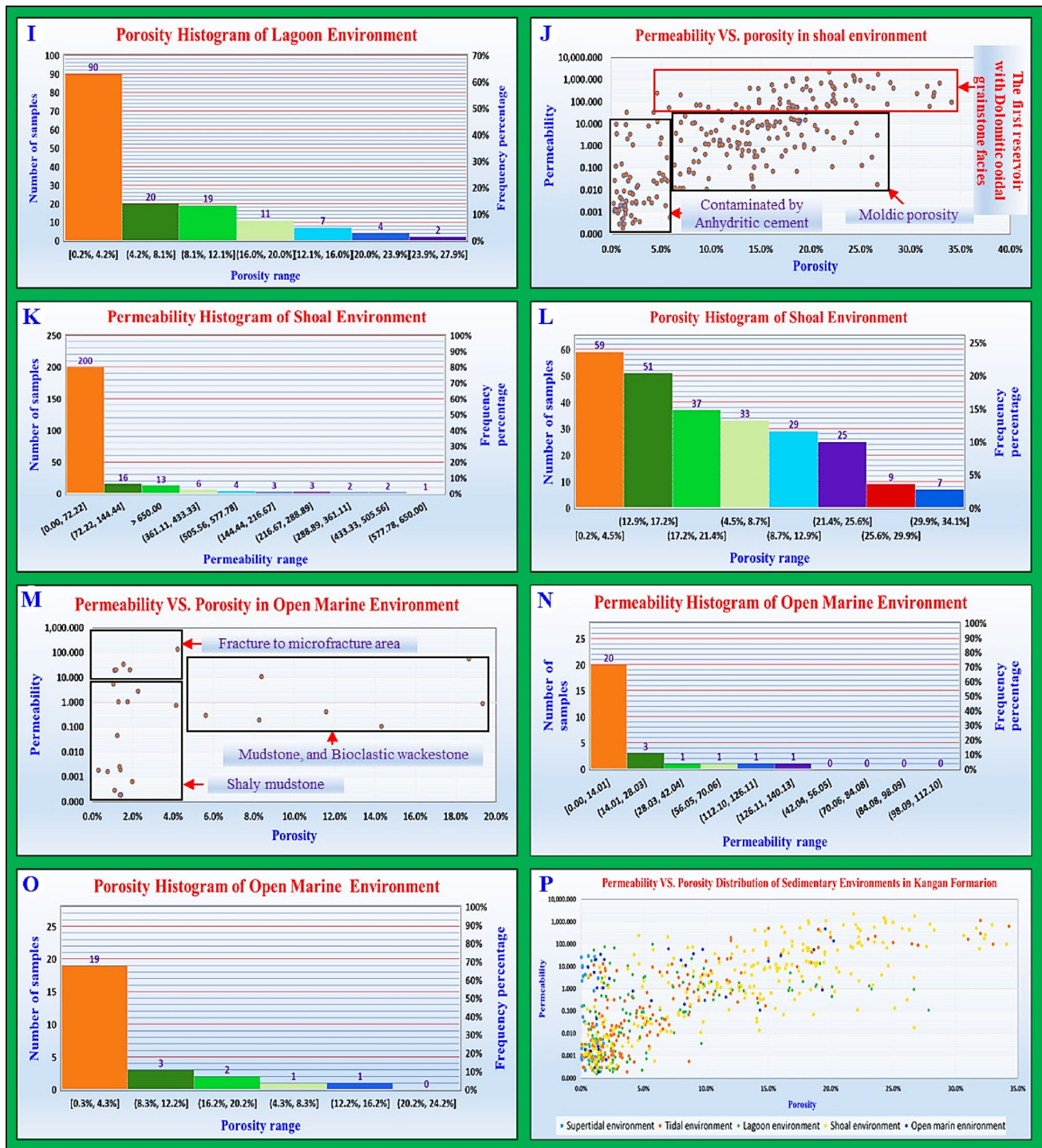


Fig. 9 Diagrams depicting permeability versus porosity and histograms for lagoon, shoal, and open marine environments, along with a comparison of the different environments within the Kangan Formation and an assessment of their reservoir quality

and oomoldic porosities. Dolomitization within the shoal environment significantly enhances reservoir quality. However, in some areas, the influence and formation of anhydrite cement can greatly reduce reservoir quality by filling the pores and creating impermeable sections. The diagram of permeability versus porosity in the shoal environment

reveals three distinct areas: (a) *Main reservoir section*: This section has a permeability range of 75–2255 mD and porosity between 8 and 34%. It is characterized by the highest reservoir quality and is considered the producible part of the reservoir (Fig. 9J). (b) *High porosity and low to medium permeability section*: In this range, porosity varies from 6.3

Table 3 Minimum, maximum, and average permeability and porosity of the facies in the Kangan formation within the study area

Facies	Permeability			Porosity		
	Average	Max	Min	Average	Max	Min
Grainstone	139.455	2,255.50	0.058	13.20%	35.10%	0.40%
Pack/Grainstone	9.603	480.15	0.018	6.30%	19.50%	0.80%
Packstone	8.841	112.98	0.01	4.30%	18.90%	0.30%
Wack/Packstone	6.495	25.38	0.001	3.20%	15.30%	0.03%
Wackestone	5.159	28.65	0.001	2.90%	9.10%	0.35%
Mudstone to Dolomudstone	4.824	32.81	0.001	4.18%	21.92%	0.008
Mudstone	4.79	48.55	0.001	2.16%	10.70%	0.12%
Muddy Anhydrite	1.5986	9.6035	0.0008	0.37%	0.80%	0.00%
Massive Anhydrite	0.017	0.17	0.0001	2.33%	8.00%	0.02%
Xln Dolostone	83.783	1,777.64	0.001	6.26%	26.73%	0.23%

to 26.7%, while permeability ranges from 0.02 to 56 mD. This section corresponds to the pelo-oid grainstone (MF9) and bioclastic intraclast ooid grainstone (MF11) microfacies. The porosities in this area are primarily moldic, intercrystalline, and to some extent intergranular, although good communication between pores is not observed (Fig. 9J). (c) *Low permeability and porosity section*: This section exhibits permeability of less than 3.4 mD and porosity below 5.6%. It includes grainstone facies where pore spaces are primarily filled with anhydrite cement in the leeward shoal environment and micritic limestone cement in the seaward shoal environment (Fig. 9J). The histogram diagram of permeability for the shoal environment indicates that the highest range shows permeabilities of 0–72 mD, associated with facies such as bioclast, intraclast, pelo-oid grainstone, as well as bioclast, intraclast, ooid grainstone (MF9 and MF11), characterized by moldic, interparticle, and intraparticle porosities (Fig. 9K). Additionally, the porosity histogram for this environment ranges from 0.2 to 4.5%, relating to grainstone microfacies with anhydrite and micritic cement (Fig. 9L).

Open marine environment

This area has an average permeability of 2.52 mD and a porosity of 1.9%, making it the lowest reservoir quality section after the supratidal zone (Table 3). The lithology of the open marine section consists of limestone, with facies ranging from mudstone to wackestone and shaly mudstone. In the context of sequence stratigraphy, the shaly mudstone microfacies in the open marine environment is identified as the *maximum flooding surface* (MFS) (Fakhar 2024). The reservoir quality in this area is typically low, with some intergranular porosity observed only at the transition from the shoal to the open marine environment. Another feature of this area is *compaction*, which is indicated by signs such as fractures and stylolites. In the open marine environment, samples exhibiting higher permeability are associated with this phenomenon of open fractures. The diagram

of permeability versus porosity for the open marine environment reveals three distinct areas: (a) *Open to semi-open fractures*: This area has a permeability range of 20.2–140.12 mD and a porosity of 1–4.2%, significantly affected by compactional diagenesis (Fig. 9M). (b) *High to medium porosity area*: This segment features porosity values from 5.6 to 19.3% and low permeability ranging from 0.11 to 56.5 mD. It corresponds to mudstone to wackestone microfacies characterized by interparticle and vuggy porosities, although there is a lack of communication between pores (Fig. 9M). (c) *Low permeability and porosity area (hardground)*: This section, consisting of shaly mudstone microfacies, has permeability of less than 5.48 mD and porosity below 4.2%. It is composed of compact and impermeable mud facies, lacking reservoir quality akin to that of the massive anhydrite found in the supratidal environment (Fig. 9M). The histogram diagram of permeability in the open marine environment indicates that the highest permeability occurs in the range of 0–14 mD, associated with bioclastic mudstone to wackestone microfacies characterized by interparticle and intraparticle porosities (Fig. 9N). Additionally, the porosity histogram for this environment ranges from 0.3 to 4.3%, corresponding to shaly mudstone microfacies. This area represents the deepest part of the Kangan Formation (Fig. 9O). The analysis of permeability to porosity across different environments of the Kangan Formation reveals that the highest reservoir quality is found in the central part of the shoal environment, characterized by the highest permeability and porosity. This area is identified as the extractable zone in the center of the Persian Gulf. Additionally, the tidal environment, featuring crystallized dolostone facies (secondary dolomite) without anhydrite cement and significant compaction, is recognized as a secondary reservoir; however, its extractable interval and reservoir quality are lower than those of the shoal environment (Fig. 9P). The permeability versus porosity diagram indicates that the lowest reservoir quality in the Kangan Formation pertains to the

supratidal, open marine, and lagoon environments, respectively (Fig. 9P).

Facies and reservoir quality

The stratigraphic and petrographic analysis underscores significant heterogeneity in reservoir potential across the Kangan Formation facies, with grainstone and dolostone exhibiting the highest abundance and favorable reservoir properties. Conversely, mudstone and wackestone microfacies demonstrate minimal contribution, reflecting their limited porosity and permeability. This variability emphasizes the critical influence of depositional environments and diagenetic processes on reservoir quality, which warrants comprehensive characterization for optimal hydrocarbon exploitation strategies (Tucker 2009; Flügel 2010). An investigation into the reservoir quality of Kangan Formation facies, utilizing petrography and core analysis, revealed that this formation can be divided into 10 distinct facies based on reservoir quality (Fig. 10). The analysis showed that mudstone, wackestone, and wack/mudstone microfacies have the lowest frequency at 4% among the Kangan Formation facies. In contrast, the highest frequencies are observed in the grainstone and dolostone microfacies, at 20% and 18%, respectively. The subsequent sections will explore the reservoir quality of these facies in greater detail.

Dolostone microfacies

Recent advances in understanding dolomitization processes suggest that the interplay between depositional environments, diagenetic conditions, and fluid flow significantly controls the heterogeneity of reservoir quality in dolostones. Autogenic dolomitization, often driven by seafloor or near-surface brines during early diagenesis, tends to produce microcrystalline, tight dolomites with low porosity and permeability. Conversely, allogenic dolomitization, associated with basinal fluid influx during deep burial, promotes larger crystal growth, cavity formation, and secondary porosity development, thereby enhancing reservoir properties (Warren 2016). This facies constitutes 18% of the Kangan Formation (Fig. 10), exhibiting an average permeability of 83.78 mD and a porosity of 6.26% (Table 3). Dolostone facies can be further divided into the following two types of microfacies. (a) *Dolostone containing primary dolomite crystals (crystal size < 20 µm)*: This facies is associated with supratidal and tidal conditions during lowstand systems tracts (lowstand system tract). Additionally, it features *pore-filling anhydrite cement* (Fig. 4F). This type of dolostone exhibits low permeability and porosity, attributed to its small, dense dolomite crystals and the presence of anhydrite. (b) *Crystallized Dolostone*: This microfacies is associated with tidal environments during transgressive systems tracts (TST) and the central regions of shoal environments (Fig. 4G). It features secondary dolomites characterized by euhedral to subhedral crystals, often formed from

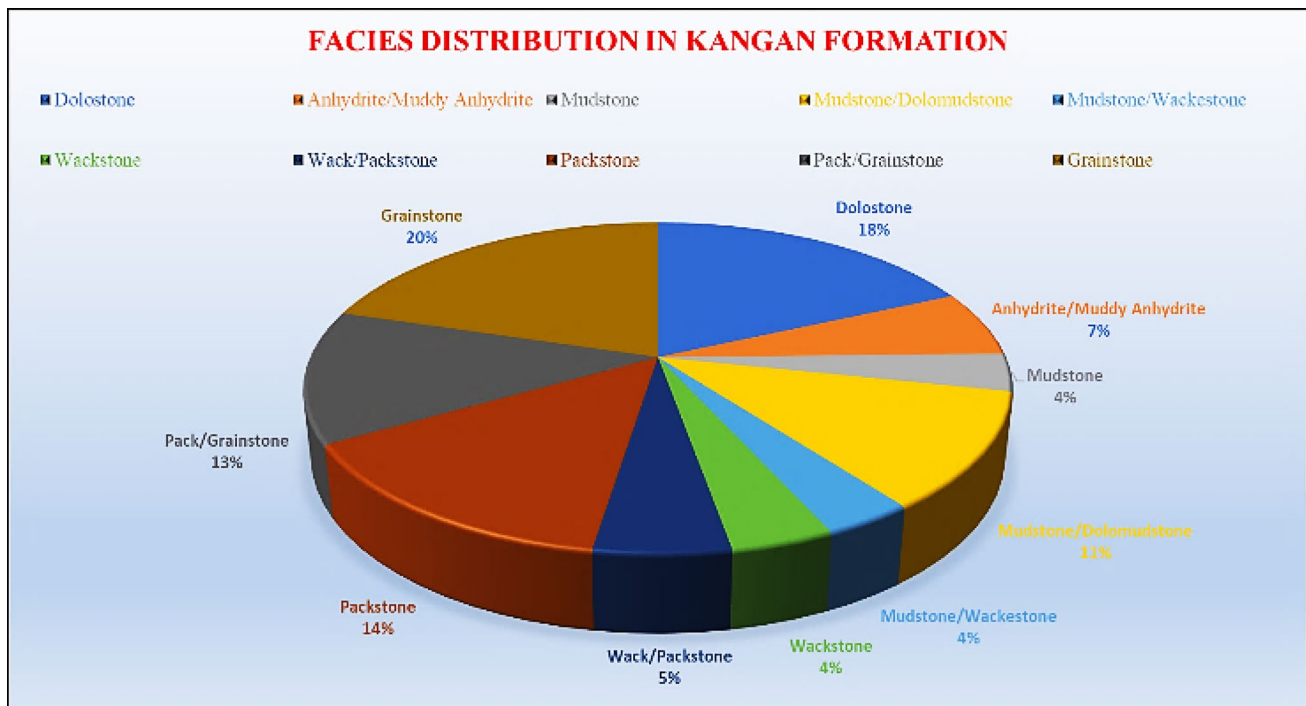


Fig. 10 Abundance of different facies of the Kangan Formation based on reservoir quality in the central part of the Persian Gulf

calcite through degrading neomorphism. The diverse permeability versus porosity distribution diagram for dolostone indicates two distinct types of dolomites, each differing in distribution, formation environments, diagenesis, and reservoir quality. Dolostone microfacies containing secondary dolomites exhibit permeability values ranging from 120 to 1770 mD and porosity between 14% and 27%, with inter-crystalline porosity, identifying them as the second reservoir of the Kangan Formation.

First Reservoir: Characterized by ooid grainstone facies in the central shoal, exhibiting permeability greater than 150 mD and porosity exceeding 25%. **Secondary reservoir:** Composed of crystalline dolostone facies in a tidal environment (TST sequence), with permeability ranging from 50 to 100 mD and porosity between 10% and 15%. Furthermore, the impermeable portion of this microfacies, characterized by very low permeability due to compression or the presence of anhydrite cement, exhibits a permeability range of 0.1 to 14 mD and a low porosity of 0.001 to 5.7% (Fig. 11A).

Massive anhydrite facies

This facies exhibits the lowest reservoir quality among all facies of the Kangan Formation, with an average permeability of 0.017 mD and a porosity of 0.023% (Table 3). The massive anhydrite facies acts as a cap rock, dividing the Kangan Formation into separate reservoir zones. The permeability versus porosity diagram indicates that this facies includes two microfacies: (a) *Primary anhydrite microfacies*: Characterized by a permeability range of 0.003 to 0.005 mD and porosity of 0.0002 to 0.006%. (b) *Recrystallized anhydrite microfacies*: Exhibiting a permeability range of 0.004 to 0.07 mD and porosity between 0.05% and 0.08%. While both types have low reservoir quality, the recrystallized anhydrite shows slightly higher permeability and porosity (Fig. 11B). In anhydrite reservoirs, diagenetic processes such as dissolution, reprecipitation, and mineral structural alterations play a pivotal role in reservoir development and enhancement. The distinction between dissolution and reprecipitation phenomena leading to the formation of secondary porosity and increased connectivity within pore networks is driven by chemical and physical responses to diagenetic conditions. These alterations not only result in variations in particle packing and fabric architecture but also significantly influence the stability and longevity of pore networks and fluid pathways. Consequently, the reservoir quality is profoundly dependent on the diagenetic history and the complexity of the processes involved (Fakhar 2024). In carbonate reservoirs, the presence and extent of anhydrite cementation significantly influence reservoir quality; pervasive anhydrite fills and cementations can obstruct pore spaces and substantially reduce permeability.

In the Permo-Triassic carbonate system of the South Pars gas field, diagenetic processes particularly dolomitization and anhydrite precipitation play a crucial role in controlling reservoir performance. Where anhydrite cementation is extensive, it often leads to pore occlusion, diminishing porosity and permeability. Conversely, areas characterized by replacive dolomitization with minimal or localized anhydrite infill tend to exhibit enhanced reservoir properties, as the development of secondary porosity and improved flow pathways occurs. The distribution, fabric-retentiveness, and timing of anhydrite formation are therefore critical factors; fabric-retentive dolomites formed under near-surface conditions preserve original depositional features, whereas fabric-destructive dolomites formed at higher temperatures and deeper burial (> 1400 m) tend to obliterate primary pore structures. A comprehensive understanding of anhydrite's spatial distribution and its diagenetic evolution is essential for optimizing hydrocarbon extraction, as the cement's heterogeneity directly influences reservoir heterogeneity and productivity potential (Rahimpour-Bonab 2010).

Muddy anhydrite facies

This anhydrite microfacies can contain up to 30% mud. This microfacies has an average permeability of 1.59mD and a porosity of 0.37% (Table 3). The permeability versus porosity diagram of this microfacies shows two areas: (a) The area has small fractures with permeability of 3.12–9.6 mD and a porosity of 0.09–0.8%, which is considered with low permeability. (b) Impermeable region with permeability of 0.0008–0.18mD and a porosity of 0.003–0.7% which has anhydrite and claystone lithology and is completely dense and impermeable (Fig. 11C).

Mudstone microfacies

Mudstone facies are critical determinants of reservoir quality, primarily influencing porosity, permeability, and heterogeneity through their role as vertical seals. Their depositional architecture shaped by paleoenvironmental factors such as braided channels controls spatial distribution and connectivity of reservoir units. Diagenetic processes, including mineral cementation and compaction, further modulate their sealing capacity and porosity evolution. Precise characterization of mudstone microfacies and diagenetic alteration is indispensable for accurate reservoir evaluation and effective development strategies (Leeder 2011). This microfacies demonstrates low reservoir quality, with an average permeability of 4.79 mD and a porosity of 2.16% (Table 3). The permeability versus porosity diagram for this facies indicates two distinct areas: (a) *Microfractured and dissolved area*: Exhibiting permeability ranging

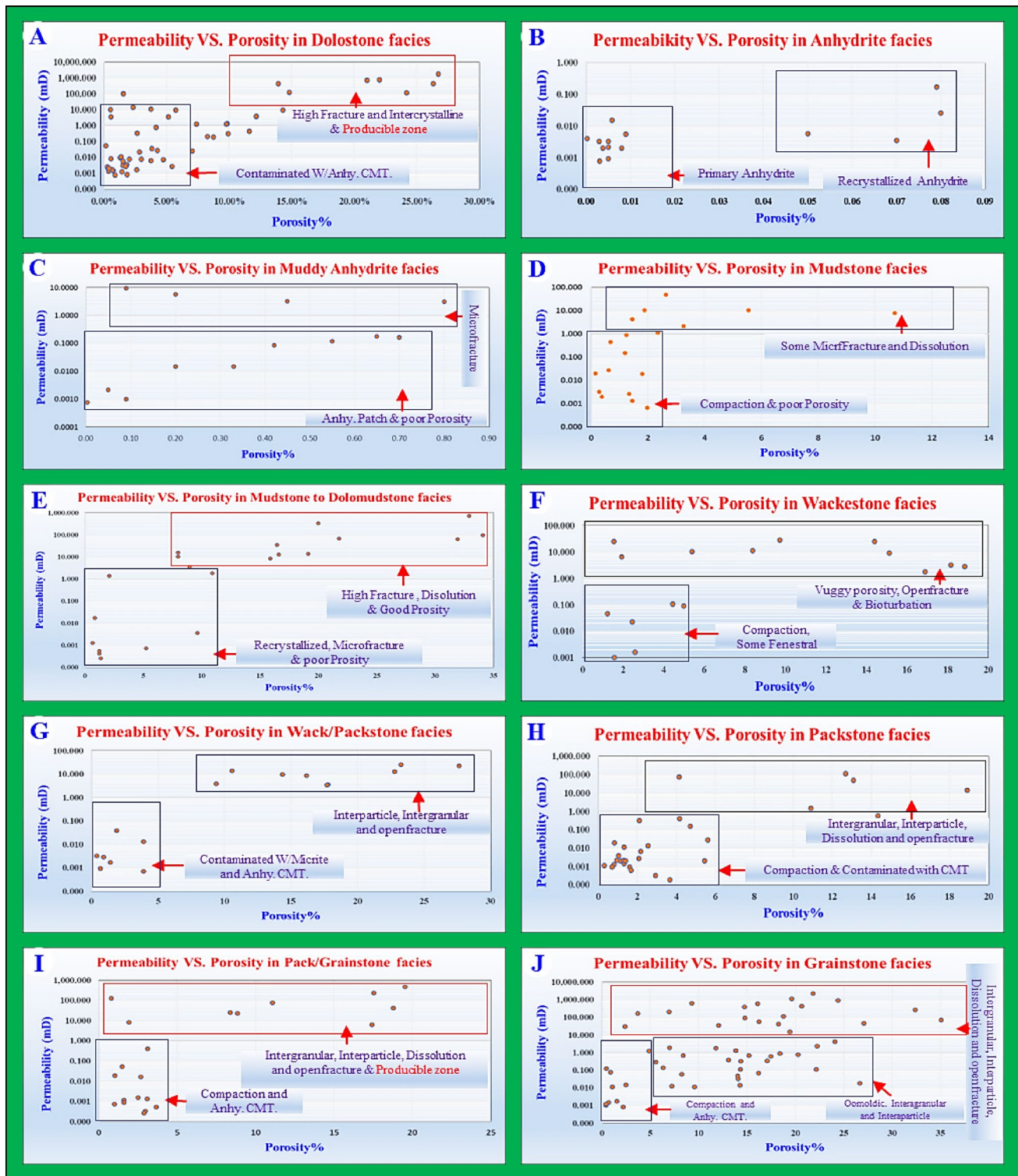


Fig. 11 Investigation of reservoir quality through permeability versus porosity diagrams for the Early Triassic facies in the central part of the Persian Gulf, utilizing core analysis and petrographic data from the study area

from 2.12 to 48.55 mD and porosity between 1.46% and 10%, which is considered low in terms of reservoir quality. (b) *Impermeable range*: Characterized by permeability of 0.001 to 1.12 mD and porosity of 0.15–2.35%, formed

in the environment of the central lagoon and influenced by compression (Fig. 11D).

Mudstone to dolomudstone microfacies

This facies constitutes 11% of the total frequency (Fig. 10), with an average permeability of 4.82 mD and a porosity of 4.18% (Table 3). Due to the presence of dolomite (up to about 50%) in this microfacies, its permeability and porosity are higher than those of the mudstone microfacies. The permeability versus porosity diagram for this facies reveals two distinct areas: (a) *Area with open fractures*: This section shows permeability ranging from 8.46 to 717.38 mD and porosity between 2.9% and 34.1%. It features open fractures and significant intercrystalline porosities; some parts of this microfacies represent the second reservoir of the Kangan Formation. (b) *Region with less micro-fracturing*: This area has a permeability range of 1.35 to 10.89 mD and porosity from 0.001 to 10.89%, exhibiting fewer micro-fractures and intercrystalline porosities. The lowest permeability and porosity in this facies are associated with compaction and some anhydrite cement, classifying it as a poorly permeable reservoir (Fig. 11E).

Wackestone microfacies

Wackestone, owing to internal-mineralogical channels and structures, plays a significant role in controlling permeability and reservoir capacity. Diagenetic processes, such as dissolution and mineral formation within these internal spaces, can cause a substantial reduction in permeability and reservoir performance, especially if these spaces are cemented with minerals or filled with sediments. Therefore, the type, amount, and diagenetic processes directly influence the quality and efficiency of the reservoir (Amel 2015). This facies constitutes 4% of the total frequency (Fig. 10), with an average permeability of 5.15 mD and an average porosity of 2.9% (Table 3). The permeability versus porosity diagram for this facies reveals two regions: (a) *Dissolved cavity porosity area*: This region has permeability ranging from 0.001 to 0.39 mD and porosity between 0.32% and 5.62%, characterized by non-effective porosity. (b) *Highly compacted area*: This section shows permeability from 0.001 to 0.1 mD and porosity between 1.23% and 4.99%, featuring some fenestral porosity and significant compaction. Anhydrite cement can be observed here as pore-filling cement (Fig. 11F).

Wackestone to Packstone microfacies

This facies comprises 5% of the total frequency (Fig. 10), with an average permeability of 6.49 mD and a porosity of 3.2% (Table 3). The permeability versus porosity diagram for this facies reveals two distinctly different areas: (a) *The area with Intergranular, fractured and open fracture*

porosities: This region exhibits a permeability range of 3.56 to 25.38 mD and a porosity between 9.37% and 27.63%. Its reservoir quality is classified as low to medium and typically unextractable. (b) *Cemented and compacted area*: This section shows a permeability range of 0.001 to 0.039 mD and porosity from 0.38 to 3.91%. It is significantly impacted by anhydrite cement, micritic cement, and compaction, resulting in low reservoir quality (Fig. 11G).

Packstone microfacies

Reservoir quality in packstone is significantly influenced by their systematically interconnected pore spaces; however, diagenetic processes and pore-filling mineralization such as anhydrite and calcite cementation can reduce porosity and permeability, thereby impacting fluid storage and flow within the reservoir (Amel 2015) is present in the text, but reference is missing in the reference section. Could you please provide the reference or delete the text citation."2015). This facies constitutes 14% of the Kangan Formation (Fig. 10), with an average permeability of 8.84 mD and an average porosity of 4.3% (Table 3). The permeability versus porosity diagram for the packstone microfacies illustrates two distinct regions: (a) *High-quality reservoir area*: This region exhibits a permeability range of 10 to 100 mD and porosity between 4% and 18%, showcasing the highest reservoir quality. The porosities in this area include intergranular, interparticle, dissolution, and open fracture porosities. (b) *Low-quality area*: This section has permeability of less than 0.1 mD and porosity of less than 4%. Due to compaction, as well as the presence of anhydrite and micritic cement, it displays the lowest reservoir quality (Fig. 11H).

Packstone to grainstone microfacies

This facies constitutes 13% of the total frequency (Fig. 10), with an average permeability of 9.6 mD and an average porosity of 6.3% (Table 3). The permeability versus porosity diagram for this facies reveals two distinct areas: (a) *High-quality reservoir area*: This region has a permeability range of 10 to 1000 mD and porosity between 5% and 20%, indicating good reservoir quality. The porosities in this area include intergranular, interparticle, dissolution, and open fracture porosity, reflecting medium to high reservoir quality, with some portions potentially being producible. (b) *Low-quality area*: This section has permeability of less than 1 mD and porosity of less than 3%. Due to compaction effects, along with the presence of anhydrite and micritic cement, it exhibits low reservoir quality (Fig. 11I).

Grainstone microfacies

Microfacies of grainstone, particularly ooid grainstone and dolomitic ooid grainstone, exhibit the highest reservoir quality due to their higher primary porosity and favorable diagenetic features. Conversely, cemented bioclastic peloidal grainstone and other microfacies with extensive cementation and compaction demonstrate poor reservoir properties. Thus, the grainstone microfacies directly influence the reservoir potential, with coarser, less cemented microfacies typically offering better permeability and storage capacity (Ibrahim 2023). These facies are the most significant reservoir facies of the Kangan Formation, comprising 20% of the total (Fig. 10), with an average permeability of 139.45 mD and an average porosity of 13.2% (Table 3). The permeability versus porosity diagram for the grainstone microfacies reveals three distinct areas: (a) *High-quality reservoir area*: This region exhibits permeability ranging from 10 to 2300 mD and porosity between 5% and 35%, showcasing the highest reservoir quality among all facies of the Kangan Formation. The porosity in this area includes intergranular, intragranular, intercrystalline, and channel porosities. (b) *Average quality reservoir area*: This region has permeability ranging from 0.1 to 10 mD and porosity between 5% and 25%, indicating average reservoir quality. The porosity types in this area include intergranular, intragranular, and moldic porosity. (c) *Low-quality area*: This section displays permeability of less than 0.1 mD and porosity of less than 3%, representing the lowest reservoir quality of this facies, characterized by anhydrite cements and compaction (Fig. 11J). The histogram diagram of permeability in these facies shows that the highest frequency is associated with the grainstone and crystallized dolostone microfacies, with frequencies of 90% and 52%, respectively. In terms of reservoir quality, these two facies contribute to the primary (grainstone microfacies) and secondary (crystallized dolostone microfacies) reservoirs in the studied succession.

The average permeability in the grainstone microfacies is 139.45 mD, while in the crystalline dolostone facies, it is 83.78 mD. Conversely, the lowest frequency of microfacies is associated with the massive anhydrite microfacies and muddy anhydrite microfacies, both of which are impermeable layers that divide the Early Triassic gas reservoirs in the central part of the Persian Gulf into distinct zones (Fig. 12A). The porosity abundance diagram indicates that the highest frequencies of porosity are found in the grainstone, packstone to grainstone, and crystallized dolostone microfacies, with frequencies of 96%, 42%, and 41.2%, respectively. In terms of porosity, these facies exhibit the highest porosity within the Kangan Formation. The grainstone microfacies has an average porosity of 13.2%, consisting of intergranular, intragranular, and oomoldic porosities.

The packstone to grainstone microfacies, with an average porosity of 6.3%, also includes intergranular, intragranular, and oomoldic porosities. The crystallized dolostone microfacies has an average porosity of 6.26%, characterized by intercrystalline porosity. In contrast, the lowest porosity values are associated with the massive anhydrite, mudstone, and muddy anhydrite facies, which have porosities of 2.33%, 2.16%, and 0.37%, respectively (Fig. 12B).

Integrated reservoir quality assessment using petrophysical parameters, facies characterization, and stratigraphic framework

Following a comprehensive facies characterization and evaluation of their reservoir quality, petrophysical data from the study area were systematically analyzed. Lithological classification was conducted by quantifying the volumetric fractions of principal components, namely dolomite (VDOL), limestone (VCALC), shale (VILL), and anhydrite (VANH). A lithology column was subsequently constructed based on these volumetric proportions to facilitate spatial interpretation. Additionally, gamma-ray spectrometry data were employed to accurately estimate shale content and its distribution within the stratigraphic interval. Gas-bearing zones were delineated through the analysis of water and gas saturation profiles derived from neutron logs, enabling precise identification of zones with potential for hydrocarbon accumulation. Petrophysical parameters including porosity and permeability were plotted against core-derived data, as illustrated in (Fig. 13; Elatrash 2021; Aftab 2023; Abdelwahhab 2024). This comparative diagram highlights the spatial distribution of various facies, encompassing high-energy tidal, intertidal, lagoonal, shoal, and open marine environments across the study area. Furthermore, the research integrates global eustatic sea-level changes within the stratigraphic framework of the sedimentary sequences, providing a comprehensive view of the depositional dynamics (Fig. 13; Posamentier 1988; Tucker 2009). Based on the integration of petrophysical diagrams, core analyses, and facies identification within the context of third and fourth-order sedimentary sequences, the study area was effectively partitioned into discrete reservoir zones. The most prominent reservoir interval corresponds to the grainstone anhydrite facies within a shoal depositional environment, followed by facies associated with dolostone deposited in tidal settings. This investigation highlights that dolomitization and dissolution diagenesis are the dominant processes responsible for enhancing reservoir quality in the region (Wang 2017; Machel 2004). Conversely, cementation, micritization, and compaction emerge as the primary diagenetic factors detrimental to reservoir performance in the

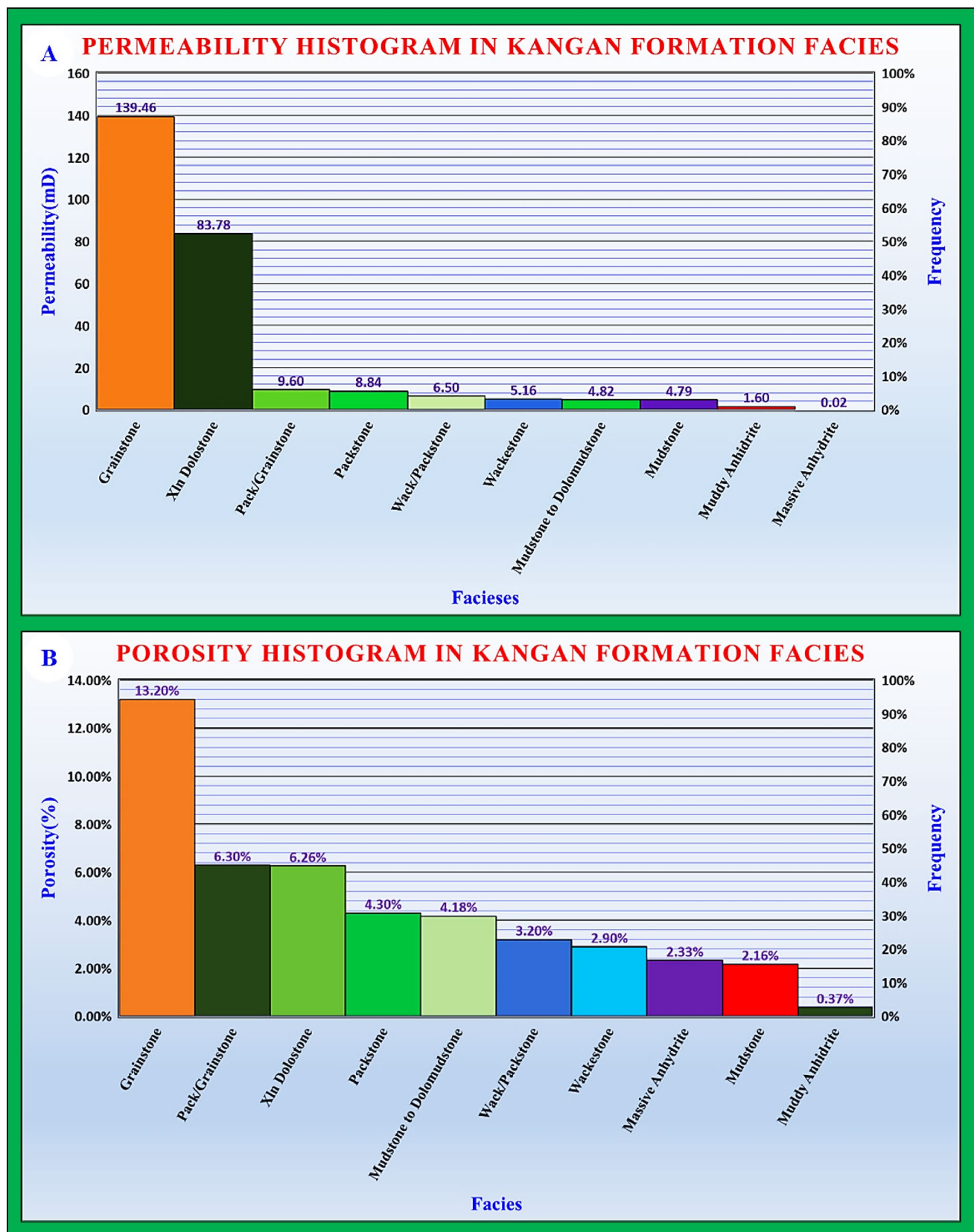


Fig. 12 Histogram of permeability and porosity in the Kangan Formation facies, based on core analysis and petrographic data from the study area

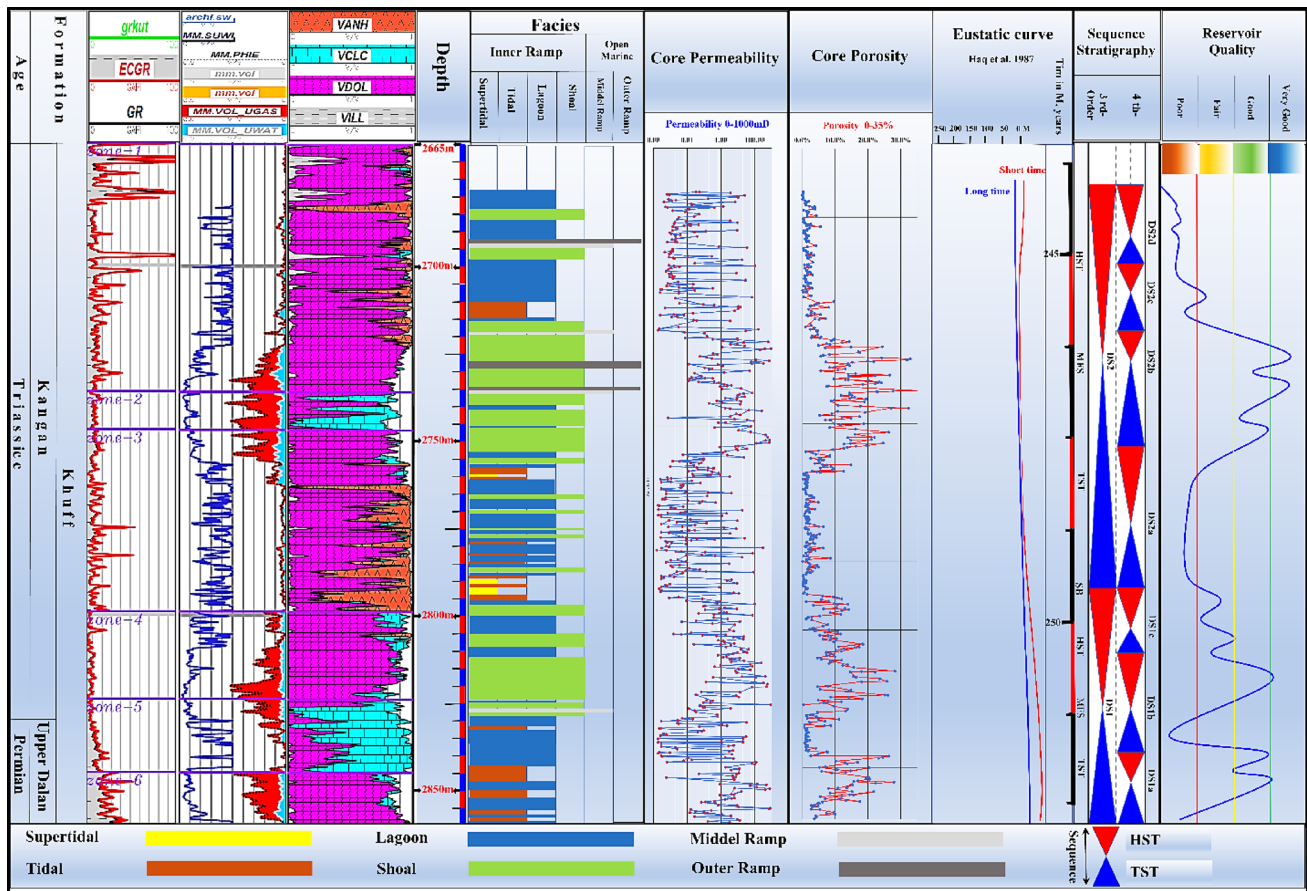


Fig. 13 Petrophysical Data Analysis, Facies Characterization, Core Analysis, Sequence Stratigraphy, Sea-Level Fluctuations, and Reser-

voir Quality Assessment of the Early Triassic in the Central Persian Gulf". (Adapted from Fakhar 2024).

Early Triassic gas accumulations, ranked according to their impact severity (Aftab2023).

Within the study area, two third-order sequences and seven fourth-order sequences were delineated. The highest reservoir quality within the third-order sequence DS1 is observed at the onset of the TST, with average permeability values ranging from 770 to 810 mD and porosity between 26% and 28%. Additionally, the beginning of the HST exhibits elevated reservoir quality, characterized by permeability values of 420 to 560 mD and porosity ranging from 25 to 28%. In the third-order sequence DS2, the most favorable reservoir conditions are identified in the distal portion of the TST, exhibiting average permeability between 430 and 750 mD and porosity from 32 to 35%. Furthermore, a smaller zone within this sequence displays high reservoir quality at the onset of the HST, with permeability ranging from 620 to 930 mD and porosity between 14% and 24% (Fig. 13; Posamentier 1988; Wang 2017). Sequence analysis indicates that optimal reservoir characteristics are associated with the shoal environment, predominantly featuring grainstone, anhydrite to grainstone, anhydrite dolomitic

facies deposited under high-energy conditions. The second key reservoir unit, with relatively narrower quality variation, corresponds to the active tidal environment, which is characterized by dolostone facies exhibiting exceptionally high intercrystalline porosity (Machel 2004; Aftab 2023).

Limitations, and suggestions for future research

Reservoir quality assessment inherently requires comprehensive sedimentological analysis, necessitating the acquisition of full core samples and subsequent core analysis. Integrating sedimentological data with petrophysical measurements and core-derived datasets yields highly precise and comprehensive reservoir characterization, facilitating accurate facies zonation and optimal hydrocarbon extraction strategies. However, this methodology is constrained by significant financial implications, primarily due to the costs associated with core retrieval and detailed core analysis, which demand complete core sampling. Additionally,

the process is time-intensive, often prolonging drilling operations and increasing operational costs. A further limitation pertains to the scarcity of specialized personnel proficient in petroleum sedimentology and petrophysics, capable of accurate interpretation of complex datasets.

It is recommended that, in each hydrocarbon field, establishing at least one deep appraisal well with a full core retrieval be prioritized. Such wells serve as fundamental reference points for reservoir quality investigations, and the resultant models can be extrapolated to other development wells within the field or adjacent reservoirs. This approach has been successfully implemented in the central Persian Gulf and the South Pars field, where zone models derived from appraisal wells have been effectively adapted to broader areas within the field, enhancing the reliability of reservoir delineation and modeling.

Conclusions

- *The shoal environment* is identified as the highest-quality reservoir zone within the studied sequence, with a frequency of 30.92%. It exhibits an average permeability of 105.6 mD and porosity of 12.5%, predominantly composed of limestone, dolomitic limestone, and dolomite. Microfacies such as grainstone and packstone to grainstone dominate, with evidence of dolomitization enhancing reservoir quality.
- The sedimentary environment, analyzed through a novel microfacies-based approach, allows *effective reservoir zoning* and facilitates the identification of carbonate reservoirs with high precision.
- *The tidal environment* ranks as the second-largest reservoir zone, comprising 32.84% of sediment volume, and exhibits moderate reservoir quality, with an average permeability of 9.34 mD and porosity of 5.3%. Notably, the microfacies mostly consist of crystallized dolostone, with permeability and porosity averaging 83.78 mD and 6.26%, respectively, primarily in energetic, shallow water zones with carbonate sand deposits.
- The reservoir quality in the tidal environment is significantly enhanced by processes such as *meteoric dissolution* and *dolomitization* via the seepage reflux model, especially in carbonate sands.
- Based on integrated microfacies, sedimentary environments, core analysis, and petrophysical data, the study delineates three *productive reservoir units*:
 1. **Crystallized Dolostone Facies:** Thickness of 9.5 m, associated with high-energy tidal zones at the Permian end.
 2. **Ooidal Grainstone Facies:** Thickness of 16 m, located in the central shoal area at the base of the Kangan Formation.
 3. **Solution-rich Microdolostone Facies:** Thickness of 17.5 m, also within the shoal's central part, affected by Mg^{2+} solutions and intense dolomitization.

- *The permeability zones* identified exhibit potential for further development and can be correlated with adjacent offshore and onshore fields in the Zagros fold belt, extending into neighboring Arab countries, highlighting their regional significance.
- This research *provides novel insights* into the sedimentary microfacies and depositional environments influencing reservoir quality, contributing to improved exploration and development strategies in carbonate hydrocarbon systems.

Declarations

Competing interests The authors declare no competing interests that may have influenced the work reported in this manuscript. There are no financial, personal, or professional relationships with individuals or organizations that could bias the content, conclusions, or publication of this research. All authors confirm that the results presented are entirely independent of any external influence.

Open Access This article is licensed under a Creative Commons Attribution-NonCommercial-NoDerivatives 4.0 International License, which permits any non-commercial use, sharing, distribution and reproduction in any medium or format, as long as you give appropriate credit to the original author(s) and the source, provide a link to the Creative Commons licence, and indicate if you modified the licensed material. You do not have permission under this licence to share adapted material derived from this article or parts of it. The images or other third party material in this article are included in the article's Creative Commons licence, unless indicated otherwise in a credit line to the material. If material is not included in the article's Creative Commons licence and your intended use is not permitted by statutory regulation or exceeds the permitted use, you will need to obtain permission directly from the copyright holder. To view a copy of this licence, visit <http://creativecommons.org/licenses/by-nc-nd/4.0/>.

References

- Abdelwahhab MA, Radwan AA, Nabawy BS, Mogren S, Ibrahim E, Leila M, Ramah M (2024) Untapped potentials exploration for deep-marine gas-bearing reservoirs: A case study from the Taranaki basin. *Mar Geophys Res* 45(3):123–145. <https://doi.org/10.1007/s11001-024-09560-5>
- Abdolmaleki J, Tavakoli V, Asadi-Eskandar A (2016) Sedimentological and diagenetic controls on reservoir qualities in the Permian–Triassic successions of Western Persian gulf, Southern Iran. *J Petrol Sci Eng* 141:90–113. <https://doi.org/10.1016/j.petrol.2016.01.020>
- Abuamarah BA, Nabawy BS (2021) A proposed classification for the reservoir quality assessment of hydrocarbon-bearing sandstone and carbonate reservoirs: A correlative study based on


- different assessment petrophysical procedures. *J Nat Gas Sci Eng* 88:103807. <https://doi.org/10.1016/j.jngse.2021.103807>
- Aftab S, Leisi A, Kadkhodaie A (2023) Reservoir petrophysical index (RPI) as a robust tool for reservoir quality assessment. *Earth Sci Inf* 16(3):2457–2473. <https://doi.org/10.1007/s12145-023-01049-w>
- Aleali M, Rahimpour-Bonab H, Moussavi-Harami R, Jahani D (2013) Environmental and sequence stratigraphic implications of anhydrite textures: A case from the lower triassic of the central Persian Gulf. *J Asian Earth Sci* 75:110–125. <https://doi.org/10.4236/ns.2013.511143>
- AlHomadhi ES (2014) New correlations of permeability and porosity versus confining pressure, cementation, and grain size, and new quantitative correlation relating permeability to porosity. *Arab J Geosci* 7:2871–2879. <https://doi.org/10.1007/s12517-013-0928-z>
- Al-Juboury AS, Al-Azzawi SF (2021) Sedimentology and reservoir characteristics of Makhmour and Zubair formations in Iraq. *Arab J Geosci* 14(19):1–15. <https://doi.org/10.1007/s12517-021-08893-8>
- Al-Khidir K, Benzagouta M, Al-Qurishi A, Al-Laboum A (2014) Integrated petrophysical parameters and petrographic analysis characterizing Khartam reservoirs of the Permo-Triassic Khuff formation, South Arabia. *J Eng Res Appl* 4(6):195–203. <https://doi.org/10.22214/ijras.2014.6327>
- Al-Maamoon AH, Askar A (2021) Reservoir properties and diagenesis of the Mujdat formation in Kuwait. *J Petrol Sci Eng* 205:108935. <https://doi.org/10.1016/j.petrol.2021.108935>
- Al-Malki AS, Mclean H (2023) Reservoir characterization of the Khuff and Saih Rawl formations in Oman. *J Nat Gas Sci Eng* 101:104592. <https://doi.org/10.1016/j.jngse.2022.104592>
- Alsharhan AS (2006) Sedimentological character and hydrocarbon parameters of the middle permian to early triassic Khuff formation, united Arab Emirates. *GeoArabia* 11:121–158. <https://doi.org/10.2113/geoarabia1103121>
- Alsharhan AS, Kendall CG, St C (2003) Sedimentary basins and petroleum geology of the Middle East. <https://doi.org/10.1007/978-94-010-0202-7>
- Alsharhan AS, Nairn AEM (1997) Sedimentary basins and petroleum geology of the middle East. Amsterdam: Elsevier. <https://doi.org/10.1016/B978-0-444-82264-0.50011-3>
- Alsharhan AS, Nairn AEM (2018) Sedimentary and petroleum geology of the upper Khaffi formation. *J Petrol Sci Eng* 164:27–40. <https://doi.org/10.1016/j.petrol.2018.01.019>
- Alsharhan AS, Nairn AEM (2019) Characteristics and hydrocarbon potential of the Thamama formation. *Mar Pet Geol* 109:295–312. <https://doi.org/10.1016/j.marpetgeo.2019.06.036>
- Al-Sharhan AS, Nairn AEM (2020) Geology and hydrocarbon potential of the permian and triassic strata in Kuwait. *GeoArabia* 25(3):159–172. <https://doi.org/10.1306/046320191927004>
- Ameen MS, Al-Khalidi A (2021) Geology and production potential of the Khuff formation in Saudi Arabia. *J Petrol Sci Eng* 203:108669. <https://doi.org/10.1016/j.petrol.2021.108669>
- Amel H, Jafarian A, Husinnec A, Koeshidayatullah A, Rudy S (2015) Microfacies, depositional environment and diagenetic evolution controls on the reservoir quality of the permian upper Dalan formation, Kish gas field, Zagros basin. *Mar Pet Geol* 57–71. <https://doi.org/10.1016/j.marpetgeo.2015.04.012>
- Bahrudi A, Talbot CJ (2003) The configuration of the basement beneath the Zagros basin. *J Pet Geol* 26(3):257–282. <https://doi.org/10.1111/j.1747-5457.2003.tb00030.x>
- Bordenave M, Hegre J (2010) Current distribution of oil and gas fields in the Zagros fold belt of Iran and contiguous offshore as the result of the petroleum systems. *Geol Soc Lond Special Publications* 291–353. <https://doi.org/10.1144/SP330.14>
- Bordenave ML (2008) The origin of the Permo-Triassic gas accumulations in the Iranian Zagros fold belt and contiguous offshore area: A review of the palaeozoic petroleum system. *J Pet Geol* 31:3–42. <https://doi.org/10.1111/j.1747-5457.2008.00405.x>
- Boughalmi S, Negra MH, Grosheny D, Éraud Y, Saidi M (2019) Reservoir qualities of turonian rudist-rich carbonates in central Tunisia (the onshore of Sfax area). *Arab J Geosci* 12(15):1–14. <https://doi.org/10.1007/s12517-019-4632-5>
- Dehghan Abnavi A, Karimian Torghabeh A, Qajar J (2021) Hydraulic flow units and ANFIS methods to predict permeability in heterogeneous carbonate reservoir: middle East gas reservoir. *Arab J Geosci*. <https://doi.org/10.1007/s12517-021-07084-5>
- Dunham R J (1962) Classification of carbonate rocks according to depositional texture. *Amer. Association Petro. Geol. Bulletin* 46(5): 1082–1114. <https://doi.org/10.1306/070618610108>
- Edwards JD, Fletcher JA (2012) Petroleum systems in the Gulf of Mexico Basin. <https://doi.org/10.1306/13211138M112356>
- Elatrash AM, Abdelwahhab MA, Wanas HA, ElNaggar SI, Elshayeb HM (2021) Multidisciplinary approach to sedimentary facies analysis of Messinian salinity crisis tectonosequences (South-Mansoura area, Nile Delta): Incised valley fill geological model reconstruction and petroleum geology-reservoir element delineation. *J Petroleum Exploration Prod Technology* 11(4):1643–1666. <https://doi.org/10.1007/s13202-021-01124-2>
- Eltom H, Abdullatif O, Babalola L, Bashari M, Yassin M, Osman MS, Abdulraziq A (2017) Integration of facies architecture, ooid granulometry and morphology for prediction of reservoir quality, lower triassic Khuff formation, Saudi Arabia. *Pet Geosci* 23(2):177–189. <https://doi.org/10.1144/petgeo2015-071>
- Esrifili-Dizaji B, Rahimpour-Bonab H (2009) Effects of depositional and diagenetic characteristics on carbonate reservoir quality: A case study from the South Pars gas field in the Persian Gulf. *Pet Geosci* 15(4):325–344. <https://doi.org/10.1144/1354-079309-817>
- Esrifili-Dizaji B, Rahimpour-Bonab H (2013a) A review of Permo-Triassic reservoir rocks in the Zagros area, SW Iran: influence of the Qatar-Fars arch. *J Pet Geol* 36(3):257–279. <https://doi.org/10.1111/jpg.12555>
- Esrifili-Dizaji B, Rahimpour-Bonab H (2013b) Carbonate reservoir rocks at giant oil and gas fields in SW Iran and the adjacent offshore: A review of stratigraphic occurrence and poro-perm characteristics. *J Pet Geol* 343–370. <https://doi.org/10.1111/jpg.12741>
- Fakhar M, Rezaee P, Karimian Torghabeh A (2022) Microfacies, depositional environment and sequence stratigraphy of the carbonate-evaporate successions of the Kangan formation in the central part of the Persian Gulf. *J Stratigraphy Sedimentology Researches Univ Isfahan* 115–146. <https://doi.org/10.22108/JSSR.2022.132142.1221>
- Fakhar M, Rezaee P, Karimian Torghabeh A (2024) Investigating the reservoir quality of the early triassic succession with a new perspective on diagenesis and sequence stratigraphy in the center of the Persian Gulf, South Pars. *J Geoenergy Sci Eng* 212367. <https://doi.org/10.1016/j.jgeo.2023.212367>
- Falcon N (1974) Southern Iran: Zagros Mountains. In A. Spencer (Ed.), *Mesozoic–Cenozoic orogenic belts* (Vol. 4, pp. 199–211). Geological Society of London, Special Publications. <https://doi.org/10.1144/GSL.SP.1974.004.01.13>
- Flügel E (2010) Microfacies of carbonate rocks. Springer. <https://doi.org/10.1007/978-3-642-03771-8>
- Gasparrini M, Bakker RJ, Bechstädt T (2006) Characterization of dolomitizing fluids in the carboniferous of the Cantabrian zone (NW Spain): A fluid-inclusion study with cryo-Raman spectroscopy. *J Sediment Res* 76(12):1304–1322. <https://doi.org/10.1306/0517067601304>
- Ghasemi M, Kakemem U, Husinnec A (2022) Automated approach to reservoir zonation: A case study from the upper permian Dalan (Khuff) carbonate ramp, Persian Gulf. *J Nat Gas Sci Eng* 97:104332. <https://doi.org/10.1016/j.jngse.2021.104332>

- Granberry RJ, Keelan DK (1977) Critical water estimates for Gulf Coast sands. Gulf Coast Association Geol Soc 27:41–43. <https://doi.org/10.1306/2F918A8B-16CE-11D7-8645000102C1865D>
- Hine AC (1977) Lily bank, bahamas; history of an active oolite sand shoal. J Sediment Res 47(4):1554–1581. <https://doi.org/10.1306/212F73B5-2B24-11D7-8648000102C1865D>
- Hossein Yar G, Rahimpour Bonab H (2011) Factors controlling the reservoir characteristics of ooid and mudstone facies of Kangan Formation in South Pars. *Journal of Stratigraphy and Sedimentology Researches*, 27, 1–16.
- Huc AY (2005) The role of sedimentology in the formation of gas reservoirs in the middle East. J Pet Geol 28(2):153–173. <https://doi.org/10.1111/j.1747-5457.2005.tb00275.x>
- I Al-Husseini M (2000) Origin of the Arabian plate structures: Amar collision and Najd rift. GeoArabia 5:527–542. <https://doi.org/10.2113/geoarabia0504527>
- Ibrahim Y, Morozov VP, Kolchugin AN, Leontev A (2023) Impact of microfacies and diagenesis on the reservoir quality of upper devonian carbonates in Southeast tatarstan, Volga-Ural basin, Russia. Petroleum Res 8:386–403. <https://doi.org/10.1016/j.ptlr.2022.10.006>
- Insalaco E, Virgone A, Courme B, Gaillot J, Kamali M, Moallemi A, Lotfipour M, Monibi S (2006) Upper Dalan member and Kangan formation between the Zagros mountains and offshore fars, iran: depositional system, biostratigraphy and stratigraphic architecture. GeoArabia 11(2):75–176. <https://doi.org/10.2113/geoarabi.110275>
- Jafarian A, Fallah-Bagdash R, Mtttern F, Heubeck C (2017) Reservoir quality along a homoclinal carbonate ramp deposit: the permian upper Dalan formation, South Pars field, Persian Gulf basin. Mar Pet Geol 88:587–604. <https://doi.org/10.1016/j.marpetgeo.2017.09.002>
- Kadkhodaie-Ilkhchi R, Nouri B, Jodeyri R (2018) Dolomitization and its relationship with sedimentary facies and reservoir quality of the upper Dalan and Kangan formations in Southeast district of the Persian Gulf. Sci Q J Geoscience (Geological Surv Iran) 231–242. <https://doi.org/10.22071/gsj.2018.58252>
- Kadkhodaie R, Sohrabi A, Jodeyri-Agahi R (2022) A syngenetic classification of anhydrite textures in carbonate reservoirs and its relationship with reservoir quality: A case study from the Permian-Triassic Dalan and Kangan formations. Carbonates Evaporites 44. <https://doi.org/10.1007/s13146-022-00790-5>
- Kakemem U, Adabi MH, Mahmoudi A, Anderskov K (2023) Sedimentology and sequence stratigraphy of automated hydraulic flow units—The Permian Upper Dalan Formation, Persian Gulf. <https://doi.org/10.1016/j.marpetgeo.2022.105965>
- Kakemem U, Jafarian A, Husinec A, Adabi MH, Mahmoudi A (2021) Facies, sequence framework, and reservoir quality along a triassic carbonate ramp: Kangan formation, South Pars field, Persian Gulf Superbasin. J Petrol Sci Eng 198:108166. <https://doi.org/10.1016/j.petrol.2020.108166>
- Karimian Torghabeh A, Qajar J, Dehghan Abnavi A (2022) Characterization of a heterogeneous carbonate reservoir by integrating electrofacies and hydraulic flow units: A case study of Kangan gas field, Zagros basin. J Petroleum Explor Prod Technol. <https://doi.org/10.1007/s13202-022-01572-4>
- Kavoosi MA, Jamali AM, Najji MR, Nematollahi R (2011) Depositional sequences of the lower triassic Kangan formation, Southwest Iran. Eur Association Geoscientists Eng. <https://doi.org/10.3997/2214-4609.20144081>
- Kendall CG, St C, Skipwith P, A D E (1969) Holocene shallow water carbonate and evaporate sediments of the Khor al bassam, Abu Dhabi, SW Persian Gulf. AAPG Bull 53:841–869. <https://doi.org/10.1306/5D25C803-16C1-11D7-8645000102C1865D>
- Kershaw S, Crasquin S, Li Y, Collin PY, Forel MB, Mu X, Baud A, Wang Y, Xie S, Maurer F, Guo L (2012) Microbialites and global environmental change around the Permian–Triassic boundary: A synthesis. Geobiology 10:25–47. <https://doi.org/10.1111/j.1472-4669.2011.00302.x>
- Khadr ZA, El-Wahed MA (2020) Facies analysis and reservoir quality of early triassic carbonate sequences. Mar Pet Geol 113:104163. <https://doi.org/10.1016/j.marpetgeo.2019.104163>
- Khatib Z, Sidi SH (2020) The geology and production potential of the North field gas reserves in Qatar. Pet Explor Dev 47(1):135–149. [https://doi.org/10.1016/S1876-3804\(20\)30013-3](https://doi.org/10.1016/S1876-3804(20)30013-3)
- Koop WJ, Stoneley R (1982) Subsidence history of the Middle East Zagros basin, Permian to recent. In P. E. Kent, M. P. Bott, D. P. McKenzie, & C. A. Williams (Eds.), *Philosophical Transactions of the Royal Society of London. Series A, Mathematical and Physical Sciences*, 301(1479), 359–379. <https://doi.org/10.1098/rsta.1982.0020>
- Leeder MR (2011) Sedimentology and sedimentary basins, 2nd edn. E-Book, Wiley-Blackwell
- León Carrera M, Barbier M, Le Ravalec M (2018) Accounting for diagenesis overprint in carbonate reservoirs using parametrization technique and optimization workflow for production data matching. J Petroleum Explor Prod Technol 8:983–997. <https://doi.org/10.1007/s13202-018-0446-3>
- Limin ZH, A O, Wen Z H O U, Zhong Y, Rui G, U O, Zhimin JIN, Yantao C, H E N (2019) Control factors of reservoir oil-bearing difference of cretaceous Mishrif formation in the H oilfield, Iraq. Pet Explor Dev 46(2):314–323. [https://doi.org/10.1016/S1876-3804\(19\)60011-X](https://doi.org/10.1016/S1876-3804(19)60011-X)
- Machel HG (2004) Concepts and models of dolomitization: a critical reappraisal. Geol Soc Lond Special Publications 235(1):7–63. <https://doi.org/10.1144/GSL.SP.2004.235.01.02>
- Mahdi TA, Aqrabi AA (2018) Role of facies diversity and Cyclicity on the reservoir quality of the mid-Cretaceous Mishrif formation in the Southern Mesopotamian basin, Iraq. Geol Soc Lond Special Publications 435(1):85–105. <https://doi.org/10.1144/SP435.19>
- Mehrabi H, Rahimpour-Bonab H, Enayati-Bidgoli AH (2015) Impact of contrasting paleoclimate on carbonate reservoir architecture: cases from arid Permo-Triassic and humid cretaceous platforms in the South and Southwestern Iran. J Petrol Sci Eng 126:262–283. <https://doi.org/10.1016/j.petrol.2014.12.020>
- Moore CH, Wade WJ (2013) *Carbonate reservoirs: Porosity and diagenesis in a sequence stratigraphic framework*. Newnes. eBook ISBN: 9780080528571
- Morad S, Ketzer JM, De Ros LF (2012) Linking diagenesis to sequence stratigraphy: An integrated tool for understanding and predicting reservoir quality distribution. In *Linking Diagenesis to Sequence Stratigraphy* (Vol. 45, pp. 1–36). Special Publication of the International Association of Sedimentologists. <https://doi.org/10.1002/9781118485347.ch1>
- Motiei H (1993) Stratigraphy of Zagros. In: Hushmandzadeh A (ed) *Treatise on the geology of Iran*. Geological Survey of Iran, p 582. (in Persian)
- Motiei H (1995) Petroleum geology of Zagros. In A. Hushmandzadeh (Eds.), *Treatise on the geology of Iran*. Geological Survey of Iran (in Persian), 1003 pp
- Murris RJ (1980) Middle east: stratigraphic evolution and oil habitat. AAPG Bull 64:597–618. <https://doi.org/10.1306/2F918A8B-16CE-11D7-8645000102C1865D>
- Nader FH, Pour-Bonab HR, Kamali MR, Peyravi M (2011) Carbon and oxygen-isotope stratigraphy: A tool for confirming sequence stratigraphy in the Early Triassic Kangan Formation, northern part of the Arabian Plate. In *European Association of Geoscientists & Engineers, Third EAGE Workshop on Arabian Plate Geology*, cp-271-00009. <https://doi.org/10.3997/2214-4609.20144052>
- Perotti CR, Carruba S, Rinaldi M, Bertozzi G, Feltre L, Rahimi M (2011) The Qatar–South Fars arch development (Arabian Platform, Persian Gulf): Insights from seismic interpretation and

- analogue modeling. In *New Frontiers in Tectonic Research - At the Midst of Plate Convergence*, 325–352. <https://doi.org/10.5772/20299>
- Petunin VV, Yin X, Tutuncu AN (2011) Porosity and permeability changes in sandstones and carbonates under stress and their correlation to rock texture. In *Canadian Unconventional Resources Conference*. <https://doi.org/10.2118/147401-MS>
- Peyravi M, Kamali M, Kalani M (2010) Depositional environments and sequence stratigraphy of the early triassic Kangan formation in the Northern part of the Persian gulf: implications for reservoir characteristics. *J Pet Geol* 371–386. <https://doi.org/10.1111/j.1747-5457.2010.00485.x>
- Pollastro P R M (2003) Total petroleum systems of the paleozoic and jurassic, greater Ghawar uplift, and adjoining provinces of central Saudi Arabia and Northern Arabian-Persian Gulf. *US Geol Surv Bull Report* 2202–H(100). <https://doi.org/10.3133/b2202H>
- Posamentier HW, Vail PR (1988) Eustatic controls on clastic deposition II—sequence and systems tract models. Book Chapter. <https://doi.org/10.2110/pec.88.01.0125>
- Rahimpour-Bonab H, Esrafil-Dizaji B, Tavakoli V (2010) Dolomitization and anhydrite precipitation in Permo-Triassic carbonates of the Southern Pars gas field, offshore iran: controls on reservoir quality. *J Pet Geol* 23(1):43–66. <https://doi.org/10.1111/j.1747-5457.2010.00463.x>
- Reijers TJA (2012) Sedimentology and diagenesis as ‘hydrocarbon exploration tools’ in the late permian Zechstein-2 carbonate member (NE Netherlands). *Geologos* 18:3 163–195. <https://doi.org/10.2478/v10118-012-0009-x>
- Sabouhi M, Rezaee P (2019) Investigation of hydraulic flow units of carbonate shoal reservoir facies of Kangan formation (Early Triassic) and its relationship with depositional environment and diagenesis. *Appl Sedimentology* 7(13):167–183. <https://doi.org/10.22084/psj.2020.19859.1218>
- Salih M, Reijmer JG, El-Husseiny A (2021) Diagenetic controls on the elastic velocity of the early triassic upper Khartam member (Khuff formation, central Saudi Arabia). *Mar Pet Geol* 104823. <https://doi.org/10.1016/j.marpetgeo.2020.104823>
- Schlager W (2005) Carbonate sedimentology and sequence stratigraphy (No. 8). *SEPM Soc for Sed Geology*
- Sepehr M, Cosgrove JW (2004) Structural framework of the Zagros Fold–Thrust belt, Iran. *Mar Pet Geol* 21:829–843. <https://doi.org/10.1016/j.marpetgeo.2003.07.006>
- Shakeri N, Rahimpour-Bonab H, Tavakoli V, Haji Kazemi E (2021) Combined effects of depositional and diagenetic processes on the distribution of rock types in the Lucia petrophysical classification system: A case study of the Dalan and Kangan formations. *J Stratigraphy Sedimentology Researches* 37(2):1–20. <https://doi.org/10.22108/jssr.2021.25404>
- Sherkati S, Letouzey J (2004) Variation of structural style and basin evolution in the central Zagros (Izeh zone and Dezful Embayment), Iran. *Mar Pet Geol* 21:535–554. <https://doi.org/10.1016/j.marpetgeo.2004.01.007>
- Steiner S, Dasgupta S, Basoni M, Al Aryani F, Noufal A, Mills C, Mandl J, Menon P, Raina I, Mosse L, Shasmal S, Hollaender F, Ali H, Al Afeefi B, Sookram N (2018) Targeting the Permo-Triassic tight gas in the Khuff: Lessons learned in the journey towards development, offshore Abu Dhabi, UAE. Paper presented at the Abu Dhabi International Petroleum Exhibition & Conference, Abu Dhabi, UAE, Paper Number: SPE-192809-MS. <https://doi.org/10.2118/192809-MS>
- Szabo F, Kheradpir A (1978) Permian and triassic stratigraphy, Zagros basin, Southwest Iran. *J Pet Geol* 1(1):69–81. <https://doi.org/10.1111/j.1747-5457.1978.tb00137.x>
- Tavakoli V (2016) The effect of post-extinction facies on reservoir compartmentalization of Kangan and Dalan formations in the central Persian Gulf. *J Stratigraphy Sedimentology Researches* 32(3):1–20. <https://doi.org/10.22108/jssr.2016.20874>
- Tomašových A (2004) Microfacies and depositional environment of an upper triassic intra-platform carbonate basin: the facies unit of the West Carpathians (Slovakia). *Facies* 50:77–105. <https://doi.org/10.1007/s10347-004-0004-y>
- Tucker ME, Wright VP (2009) Carbonate sedimentology. Wiley. <https://doi.org/10.1002/9781118689993>
- Wang P, Jiang Z, Yin L, Chen L, Li Z, Zhang C, Huang P (2017) Lithofacies classification and its effect on pore structure of the cambrian marine shale in the upper Yangtze platform, South china: evidence from FE-SEM and gas adsorption analysis. *J Petrol Sci Eng* 156:307–321. <https://doi.org/10.1016/j.petrol.2017.06.011>
- Warner MD, Howell RD (2010) An overview of the geology of the Arab basin with a focus on the upper jurassic. <https://doi.org/10.1016/j.pgeola.2009.10.002>. to Lower Cretaceous
- Warren JK (2006) *Evaporites: Sediments, resources and hydrocarbons*. Springer Verlag. <https://doi.org/10.1007/3-540-32344-9>
- Warren JK (2016) *Evaporites: A geological compendium*. Springer
- Wenju SUN, Zhanfeng Q I A O, Guanming SH, A O, Xiaowei S, U N, Jixian GAO, Peng CAO, Zhang J, Wangang C, H E N (2020) Sedimentary and reservoir architectures of MB1-2 sub-member of middle cretaceous Mishrif formation of Halfaya oil field in Iraq. *Pet Explor Dev* 47(4):762–772. [https://doi.org/10.1016/S1876-3804\(20\)60091-X](https://doi.org/10.1016/S1876-3804(20)60091-X)
- Wilson BR (1975) Carbonate facies in geological history. Springer, Berlin. <https://doi.org/10.1007/978-1-4612-6383-8>
- Xu Z-Y, Lin T-F, Feng M-S, Li J, Li X, Wang X-L, Yang P-G (2022) Tidal channel sedimentary characteristics and reservoir distribution of carbonate, W Field in the Middle East. In *Springer series in geomechanics and geoengineering* (pp.325–333). https://doi.org/10.1007/978-981-19-2149-0_29
- Zadvinskikh A, Harke M, Zafarani H (2019) Geological features of the Kangan formation in the Persian Gulf region. *Energy Sour Part A Recover Utilization Environ Eff* 41(13):1603–1615. <https://doi.org/10.1080/15567036.2019.1612371>
- Ziegler MA (2001) Late permian to holocene paleofacies evolution of the Arabian plate and its hydrocarbon occurrences. *GeoArabia* 6(3):445–504. <https://doi.org/10.1144/geoarabia.6.3.445>

Publisher's note Springer Nature remains neutral with regard to jurisdictional claims in published maps and institutional affiliations.

Authors and Affiliations

Majid Fakhar¹ · Payman Rezaee¹ · Amir Karimian Torghabeh^{2,3,4} 

✉ Payman Rezaee
p.rezaee@hormozgan.ac.ir

✉ Amir Karimian Torghabeh
amirkarimian@shirazu.ac.ir

Majid Fakhar
m.fakhar.phd@hormozgan.ac.ir

¹ Department of Geology, Faculty of Basic Sciences,
University of Hormozgan, Bandar Abbas, Iran

² Department of Earth sciences, Faculty of sciences, Shiraz
University, Shiraz, Iran

³ Fossil Energy Technologies Development Research Center,
Shiraz University, Shiraz, Iran

⁴ Department of Geology, Faculty of Sciences, Ferdowsi
University of Mashhad, Mashhad, Iran